

CE5516 Civil Engineering Dissertation

Department of
Civil and Environmental Engineering
Brunel University London

Final Report

MSc in Structural Engineering

2017-2018

Name: Mirko Fernando Flores Jimenez

Student ID: 1739320

Title: "Numerical analysis and experimental correlation of uncoupled concrete walls incorporating Shear Link Bozzo connections"

Supervisor: Dr Theodosios Papathanasiou

Abstract

This project presents an analytical comparison between an experimental test and a numerical model of uncoupled concrete walls using Shear Link Bozzo (SLB) connections. The purpose of this project is to analyse the influence of the different parameters in the behaviour of the SLB connections and how to improve their performance.

Concrete structural systems are well known worldwide due to their stiffness; however, their lack of dissipative capacity has caused many catastrophes. Dr Luis Bozzo came with the idea of taking advantage of the dissipative capacity of metallic steel connections; therefore, he developed a dissipator called SLB connection that allows to combine different features of the structural systems mentioned in order to create a system that presents rigidity, flexibility and ductility at the same time.

In order to understand the structural behaviour of the SLB connections, some tests of uncoupled concrete walls applying this innovative system were performed at National Autonomous University of Mexico. These tests results are used to validate their numerical simulations through a Finite Element Analysis software; in this case, ABAQUS CAE. Once validated, the main parameters of the SLB connections are varied to obtain how these affect their general behaviour.

The results have shown that increasing or decreasing the volume of the SLB connections improves or deteriorates their behaviour respectively; however, the most effective and beneficial approach is to enhance the connection between the SLB connections and reaction concrete wall.

Acknowledgements

I would first like to thank my thesis advisor Dr Theodosios Papathanasiou of the Department of Mechanical, Aerospace and Civil Engineering at Brunel University London. His office was always open whenever I got in trouble or had a question about my project. He consistently allowed this research to be my own work, but steered me in the right the direction whenever he thought I needed it.

I would also like to thank the experts who were involved since the beginnings of this research project: Dr Luis Bozzo and Dr Hector Guerrero. Without their passionate participation and input, the developing of this research could not have been conducted.

Finally, I must express my very profound gratitude to my family for providing me with support and continuous encouragement throughout this year of study and through the process of researching and writing this thesis. This accomplishment would not have been possible without them. Thank you.

Table of contents

| | |
|--|----|
| 1. List of notations | 6 |
| 2. Lists of tables | 7 |
| 3. Lists of figures | 8 |
| 4. Introduction | 10 |
| 4.1. Justification | 10 |
| 4.2. Aim and objectives | 11 |
| 4.2.1. Main aim..... | 11 |
| 4.2.2. Objectives | 11 |
| 4.3. Methodology | 11 |
| 5. Literature review | 11 |
| 5.1. Modern systems of seismic protections | 11 |
| 5.1.1. Active control systems | 12 |
| 5.1.2. Hybrid control systems..... | 12 |
| 5.1.3. Semi active control systems | 12 |
| 5.1.4. Passive control systems | 12 |
| 5.1.4.1. Passive control using Base Isolation | 13 |
| 5.1.4.2. Passive control using Tuned Mass Dampers..... | 13 |
| 5.1.4.3. Passive control using Energy Dissipators..... | 13 |
| 5.2. Passive Dissipators of Energy | 14 |
| 5.3. Dissipators based on Metal plastification..... | 14 |
| 5.3.1. Dissipators based on bending | 15 |
| 5.3.2. Dissipators based on shear..... | 16 |
| 5.3.3. Dissipators based on metal extrusion..... | 17 |
| 5.4. SLB Connections | 17 |
| 5.4.1. The conception of the idea | 17 |
| 5.4.2. First researches | 18 |
| 5.4.3. Experimental tests and numerical models..... | 19 |
| 5.4.4. Mathematical models | 20 |
| 5.4.5. Geometry and Manufacturing process | 22 |
| 5.4.6. Design tables..... | 23 |
| 6. Test setup | 23 |
| 6.1. SLB connections | 23 |
| 6.2. Concrete Frame | 25 |

| | | |
|----------|--|-----------|
| 6.3. | Instrumentation | 26 |
| 6.4. | Loading pattern | 27 |
| 6.5. | Experimental results..... | 28 |
| 6.5.1. | Hysteresis curves | 28 |
| 6.5.1.1. | Frame without SLB connections under monotonic cyclic load | 28 |
| 6.5.1.2. | Frame with SLB connections type 1 under monotonic cyclic load | 29 |
| 6.5.1.3. | Frame with SLB connections type 2 under monotonic cyclic load | 29 |
| 7. | FEA modelling | 30 |
| 7.1. | Mesh discretization | 30 |
| 7.2. | Material properties..... | 31 |
| 7.2.1. | Constitutive model of reinforcing bar steel..... | 31 |
| 7.2.2. | Constitutive model of SLB connection steel | 31 |
| 7.2.3. | Constitutive model of reinforced concrete | 32 |
| 7.3. | Loading pattern | 33 |
| 7.4. | Boundary conditions..... | 34 |
| 7.5. | Validation | 35 |
| 7.5.1. | Concrete frame without SLB connections..... | 35 |
| 7.5.2. | Uncoupled frame with SLB connections type 1 | 36 |
| 8. | Influence of parameters | 37 |
| 8.1. | Influence of Total height, dissipative height, width, and dissipative thickness..... | 38 |
| 8.2. | Influence of horizontal position of SLB connections..... | 38 |
| 8.3. | Fixed supports..... | 39 |
| 9. | Results and discussions | 39 |
| 9.1.1. | Concrete frame without SLB connections..... | 39 |
| 9.1.2. | Uncoupled frame with SLB connections type 1 | 40 |
| 9.1.3. | Uncoupled frame with SLB connections type 2 | 40 |
| 10. | Conclusions and Recommendations | 40 |
| 10.1. | Conclusions | 40 |
| 10.2. | Recommendations for further action | 41 |
| | Appendix A: Engineering Simulation..... | 44 |
| | Appendix B: Mesh sensitivity | 45 |
| | Appendix C: Von Mises stress distribution in all studied specimens. | 46 |

1. List of notations

| | |
|-------------|----------------------------------|
| K_1 | Initial stiffness |
| K_2 | Post-yielding stiffness |
| d_y | Initial yielding displacement |
| f_y | Initial yielding force |
| D_y | Yield displacement |
| F_y | Yield force |
| F_{max} | Maximum force |
| D_a | Web buckling displacement |
| e | Milled area thickness |
| E_d | Dissipated energy |
| k_d | Diagonal stiffness |
| A_d | Diagonal area |
| E | Young's modulus |
| k_w | Window stiffness |
| G | Shear modulus |
| A | Area |
| h | Height |
| k_r | Stiffness of the thicker section |
| I | Second moment of area |
| F | Applied force |
| F_w | Force in windows |
| F_r | Force in thicker section |
| x_w | Window displacement |
| x_r | Displacement of the thicker area |
| k_{diss1} | Stiffness before yielding load |
| k_{diss2} | Stiffness after yielding load |

2. Lists of tables

| | |
|--|----|
| Table 1. Experimental values for the considered main parameters (Cahis, et al., 2000) | 19 |
| Table 2. Selection criteria for the dimensions of the dissipators (Hurtado & Bozzo, 2008) | 20 |
| Table 3. The most relevant design parameters for the devices (Hurtado & Bozzo, 2008) | 24 |
| Table 4. Concrete damage plasticity parameters (Dassault Systèmes Simulia Corp., 2010). | 33 |
| Table 5. Spring Stiffness | 34 |
| Table 6. Parameters variation..... | 38 |
| Table 7. Von Mises stress distribution in all specimens (Time interval: 25 sec)..... | 46 |
| Table 8. Von Mises stress distribution in all specimens (Time interval: 28 sec)..... | 47 |

3. Lists of figures

| | |
|--|----|
| Figure 1. (a) Conventional structure. (b) Seismic isolated structure (Verma, et al., 2017). | 13 |
| Figure 2. ADAS device (De la Llera, 2010) | 15 |
| Figure 3. TADAS device (Chambilla, 2015) | 16 |
| Figure 4. Honey-Comb device (Chambilla, 2015) | 16 |
| Figure 5. Shear panel arrangement (Oviedo, 2008) | 16 |
| Figure 6. Dissipator by lead extrusion (Cahis, 2000) | 17 |
| Figure 7. (a) A-device before and after web damage occurs. (b) Maximum cycle vertical force (semi-sum) versus displacement in the four devices. (Cahis, et al., 2000) | 19 |
| Figure 8. Analytical scheme of the composed system diagonal + SL device (Nuzzo, et al., 2015). | 21 |
| Figure 9. (a) Force-displacement diagram of the SL device. (b) Force-displacement diagram of the diagonal structure. (c) Force-displacement diagram of the Diagonal + SL device (Nuzzo, et al., 2015). | 22 |
| Figure 10. Dimensions for the Disip4SL30_2 device (Hurtado & Bozzo, 2008) | 23 |
| Figure 11. (a) Dimensions of SLB connection type 1. (b) SLB connection type 1. (c) Dimensions of SLB connection type 2. (d) SLB connection type 2 (Instituto de Ingenieria UNAM, 2017). | 25 |
| Figure 12. Reinforced concrete frame used in the test (Instituto de Ingenieria UNAM, 2017) | 26 |
| Figure 13. Dimensions (mm) of the reinforced concrete frame. (Instituto de Ingenieria UNAM, 2017). | 26 |
| Figure 14. (a) Instruments location. (b) CDPs location. (Instituto de Ingenieria UNAM, 2017) | 27 |
| Figure 15. (a) Leds location. (b) Leds in the test setup. (Instituto de Ingenieria UNAM, 2017) | 27 |
| Figure 16. Pattern of applied displacements. | 28 |
| Figure 17. (a) Hysteresis curve – Frame without SLB connections. (b) Hysteresis curve envelop - Frame without SLB connections. (Instituto de Ingenieria UNAM, 2017). | 28 |
| Figure 18. (a) Hysteresis curve – Frame with SLB connections type 1. (b) Hysteresis curve envelop – Frame with SLB connections type 1 (Instituto de Ingenieria UNAM, 2017). | 29 |
| Figure 19. (a) Hysteresis curve – Frame with SLB connections type 1. (b) Hysteresis curve envelop – Frame with SLB connections type 1 (Instituto de Ingenieria UNAM, 2017). | 29 |
| Figure 20. Mesh configuration of FE model of the test. | 30 |
| Figure 21. Elastic-perfectly plastic behaviour of steel bars (Broujerdian, 2016). | 31 |

| | |
|--|----|
| Figure 22. Structural steel A36 stress - strain curve (The Materials Information Society, 2002)..... | 32 |
| Figure 23. (a) Tension behaviour associated with tension stiffening. (b) Compressive behaviour associated with compression hardening (Dassault Systèmes Simulia Corp., 2010). | 33 |
| Figure 24. Adjusted loading pattern - numerical model..... | 34 |
| Figure 25. Springs position | 35 |
| Figure 26. Load-Displacement relationship of "Concrete frame without SLB connections" (Experimental test) | 35 |
| Figure 27. Load-Displacement relationship of "Concrete frame without SLB connections" (Experimental test – Numerical modelling)..... | 36 |
| Figure 28. Force - Displacement relationship of SLB connections type 1..... | 37 |
| Figure 29. Von Misses stresses for the SLB connection Type 1..... | 37 |
| Figure 30. Influence of different parameters – numerical models (%) | 38 |
| Figure 31. Influence of position – numerical models..... | 39 |
| Figure 32. Load-Displacement relationship (Numerical model – spring supports / fixed supports) | 39 |
| Figure 33. Mesh distribution comparison..... | 45 |
| Figure 34. Von Mises tress distribution - finer mesh in steel elements..... | 45 |

4. Introduction

4.1. Justification

In some seismic and developing countries, it is necessary to find a way to construct buildings that will stand strong earthquakes and at the same time will be cost efficient. Many devices have been developed in the last decades like seismic isolators and dissipators applied mainly to structures of high importance. These devices are characterized by their capacity to dissipate energy while deforming. Due to their high cost, they are available only for governmental or private structures where resources allow to use different ways to minimize the effects of earthquakes.

However, it is still of great importance to develop devices that will allow small structures to mitigate earthquake motions, in which the price will be a critical factor.

The SLB connections are characterized by their capacity to absorb high amount of energy and their relatively low cost. This modern device might be the solution for the small housing under seismic forces, as well as for tall buildings.

Experimental tests have been executed at the Structures Lab of the Engineering Institute of the National Autonomous University of Mexico at the request of “Luis Bozzo Structures and Projects S.L.”. Three experimental tests were performed of uncoupled concrete walls incorporating SLB connections in October 2017.

The tests consisted of a concrete frame without using SLB connections, another using the same concrete frame using two SLB connections with a design capacity of 125 kN each; and an additional test of the concrete frame using two SLB connections with a design capacity 250 kN each. The same loading pattern was used in the three tests which was controlled through displacements and applied quasi statically.

The next task undertaken in this research is to correlate the results gotten by the experimental tests with numerical models which will represent the behaviour of the structure under monotonic quasi static loads through the employment of a finite element analysis software; ABAQUS CAE was chosen in order to simulate the test behaviour.

Once the numerical simulation is validated using the experimental results, varying several parameters such as the total height, dissipative height, width, thickness, position, dimension of the dissipators, and others will allow to study how each of this parameters can be employed more effectively leading to better results.

4.2. Aim and objectives

4.2.1. Main aim

- Validate the numerical models with experimental test of uncoupled concrete walls incorporating SLB connections.

4.2.2. Objectives

- Analyse the influence of geometrical parameters such as the total height, dissipative height, width and dissipative thickness.
- Analyse the influence of the horizontal position of the SLB connections on their performance.
- Analyse the influence of different types of supports on the behaviour of the SLB connections.

4.3. Methodology

In order to validate the numerical model, it was necessary to analyse the results given by the experimental tests. All the structural elements were modelled using AUTOCAD and ABAQUS CAE; concrete elements such as columns and beams, and steel reinforcement were model using ABAQUS due to its simple geometry; on the other hand, structural steel elements such as plates and SLB connections were modelled using AUTOCAD due to their complex geometry and its manufacturing process requirement to work as a unit. General user concepts of the software are presented in Appendix A.

Different constitutive models were used to accurately reproduce the experimental tests. The concrete elements which are part of the frame were modelled separately in order to get its independent behaviour. After reaching similar values as the experimental test using just the concrete frame, SLB connections were added to the numerical model.

Once the results of the whole structure are validated properly, an analysis iterating different parameters of the SLB connections is performed in order to get an idea of the most influencing parameters.

5. Literature review

5.1. Modern systems of seismic protections

Building performance, according to the traditional approach of seismic resistant design, is based in the capacity of the structure to dissipate the energy generated by earthquakes through a combination of known properties such as ductility, resistance and rigidity.

It is expected that the structure behaves elastically under minor seismic forces and inelastically when is subject to moderate and severe seismic forces. This inelastic behaviour is characterized by energy dissipation through no recoverable deformations which aggravates as drift increases and has important consequences of considerable structural and non-structural damage.

There are innovative solutions with respect to structural vibrations produced by earthquakes. These structural systems use alternative methods in order to diminish internal forces of structures, thus improving its dynamic characteristics based in passive, active, semi-active and hybrid control approaches (Boza & Galan, 2013).

5.1.1. Active control systems

These structural systems are characterized by the use of actuators, sensors inside the structure and part-time controllers. Actuators are utilized to counteract directly seismic forces imposed to structures; and the sensors and control systems are in charge of measuring the counteracting force to be applied. However, the complexity of the algorithms used in this system and the amount of energy applied make this system less attractive (Cahis 2000, as cited in Chambilla 2015).

5.1.2. Hybrid control systems

This system is the combination of active and passive systems. Consequently, it is possible to obtain improvements with respect to the active system since energy consumption of the system is decreased. Besides, the functionality of the system is not affected if somehow the sensors stop working because the passive system will be working constantly. Hybrid systems that have woken the highest interest value among experts are the Hybrid Mass Damper (HMD) and Based Isolation with active displacement control (Cahis 2000, as cited in Chambilla, 2015).

5.1.3. Semi active control systems

The functioning of these systems is similar to active ones except of its reactive behaviour under seismic forces. The devices utilized are the same ones used in passive systems combined with actuators that allow to modify dynamic properties of the structure to low levels of energy consumption (Oviedo, 2008).

5.1.4. Passive control systems

These systems are based on mechanically simple devices which respond inertially under seismic actions and, unlike the rest, are less expensive and do not depend of external sources of energy to work.

The passive devices display reactive behaviour and their response is not controllable depending uniquely on working conditions. These devices interfere altering dynamic properties of the building, provoking a considerable reduction of the structural response. (Oviedo, 2008).

These systems can be classified in Base Isolation, Energy Dissipation, and Tuned Mass Damper systems:

5.1.4.1. Passive control using Base Isolation

Base Isolation is a design approach which is based on the uncoupling of the structure from the ground movement to protect the previous from seismic effects. This is possible through the use of flexible devices to horizontal movement and rigid to vertical displacement located among the foundations and superstructure. These devices increase the fundamental period of the structure uncoupling it from the ground movement and limiting the energy input from external sources (Oviedo, 2008).

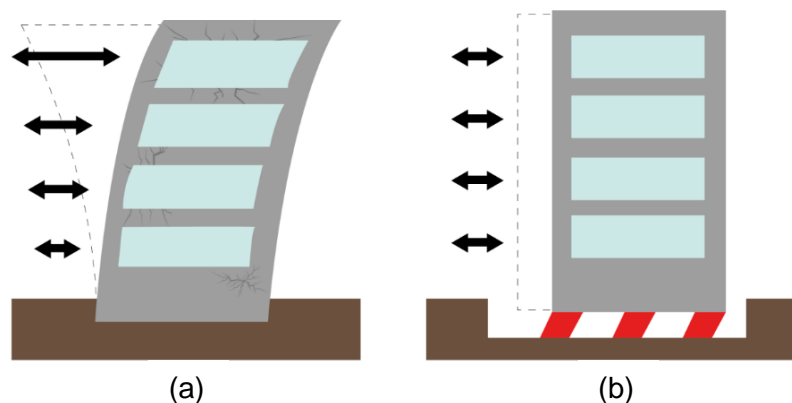


Figure 1. (a) Conventional structure. (b) Seismic isolated structure (Verma, et al., 2017).

5.1.4.2. Passive control using Tuned Mass Dampers

The Tuned Mass Dampers (TMD) insert to the structure, generally on upper floors, a constitutive system of one degree of freedom composed by a mass which is a restitutive element and a damping mechanism. In order to reduce the dynamic response of the TMD, its oscillation frequency must be equal to the fundamental frequency of the structure.

Its main drawback is that it requires a large amount of mass and an important space availability for its installation (Oviedo, 2008).

5.1.4.3. Passive control using Energy Dissipators

On the other hand, energy dissipators do not alter input energy and display efficiency while dissipating important amount of seismic energy avoiding this to be dissipated by inelastic deformation from structural elements.

Energy dissipators present several advantages such as:

- Reduction of damage level in structures and energy concentration in additional devices which are identified and easy to replace.
- Reduction of shear forces, accelerations and drifts; therefore, less damage is provoked in structural and non-structural elements. In many cases, structures keep behaving elastically.
- Energy Dissipators can meet high architectural requirements since they allow to use large spaces as well as use of new material for non-structural elements, and provide comfort and safety to users.
- Energy Dissipators are not just utilized to control seismic forces, they are also used to control vibrations caused by winds and military implementations.

5.2. Passive Dissipators of Energy

The energy dissipators minimize input seismic energy through inelastic deformations, maximizing the damping capacity of the structure (Oviedo, 2008). Energy dissipators are classified either hysteretic or viscoelastic.

Hysteretic energy dissipators are based on:

- Metal Plastification due to bending, shear or extrusion.
- Friction among surfaces.

Viscoelastic energy dissipators are based on:

- Viscoelastic solids.
- Viscoelastic fluids.

5.3. Dissipators based on Metal plastification

Metal Plastification in energy dissipators can be produced through structural stresses or extrusion processes. Any load, such as torsion, flexion, shear or axial can lead to metal plastification processes. Steel has been the most utilized material for this purpose. Among its main advantages, it is its ease of machining and weldability; besides, its low cost and high ductility level. In order to reduce the structural response, it is preferable to dissipate energy since low strength and displacement intervals. Hence, several tests have been executed using dissipators made of low elastic levels and high deformation capacity related to conventional structural steel. These energy dissipators are based on plastification due to shear stress, resulting in high stiffness devices and plastification stresses from reduced values of deformations and high uniformity in plastic deformation distribution (Cahis 2000, as cited in Chambilla, 2015).

5.3.1. Dissipators based on bending

There are several devices that plastify by flexion. The behaviour of two U-shaped plates which dissipate energy by pure flexion while rolling due to relative displacement among its ends have been studied (Cahis 2000, as cited in Chambilla, 2015).

One of the most studied and well-known devices is called ADAS (Adding Damping and Stiffness), which is a device composed of a combination of steel plates with constant thickness and variable X shape. The number of parallel steel plates is variable, allowing to adjust the dissipator according to structural design requirements.

Each plate of the device is restricted to rotate in both ends, consequently, perpendicular relative displacements between them towards the plane of the plate produce a linear, symmetric and with double curvature distribution of bending moments.

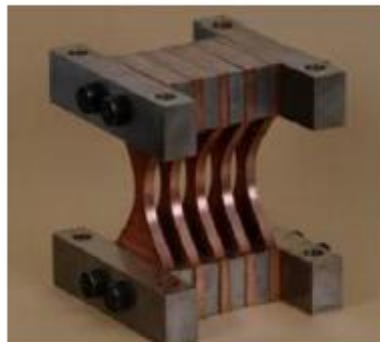


Figure 2. ADAS device (De la Llera, 2010)

The device shown in Figure 3 is known as TADAS system. Likewise ADAS, it is composed of trapezoidal parallel steel plates of constant thickness. Since its plates are fixed in one end and pinned in the other, a global plastification distribution is possible. With a relative displacement between both ends of the plate perpendicular to its plane, it is possible to obtain bending plastification due to simple curvature. While applying this system to steel frames, similar responses to structures applying ADAS system were obtained.

Besides, a device made of a mechanized steel layer due to empty spaces among dissipators is known as Honeycomb. Its geometry has the objective to achieve a uniform plastification. Its hysteretic behaviour is very stable and almost rectangular, with a close response to the rigid-plastic displayed by the ADAS device, which is more flexible.



Figure 3. TADAS device (*Chambilla, 2015*)



Figure 4. Honey-Comb device (*Chambilla, 2015*)

5.3.2. Dissipators based on shear

The majority of these dissipators adopt a T-shaped geometry with rigid web. This system displays high ductility, and allows stable hysteretic cycles.

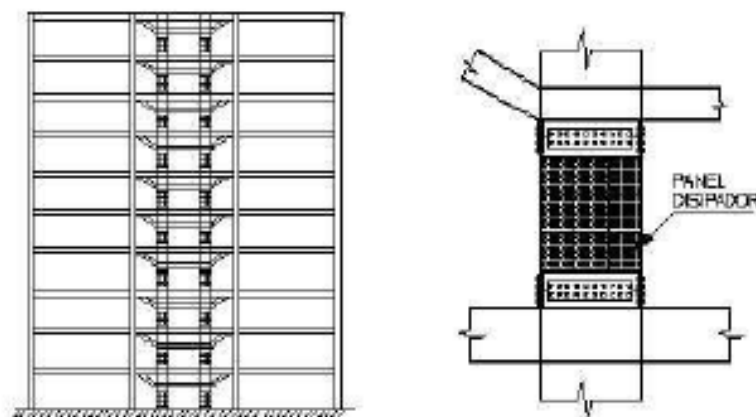


Figure 5. Shear panel arrangement (*Oviedo, 2008*)

The shear panels are rigid steel plates. Their structure, with distant stiffeners, forces to use large thicknesses to avoid buckling. High ductility steels with low elastic limit are convenient to allow large thicknesses in order to meet shear stresses, with an inferior necessity of stiffening (Oviedo, 2008).

5.3.3. Dissipators based on metal extrusion

The PVD (Penguin Vibration Damper) was designed in 1976, which dissipates energy by lead extrusion. In figure 6, the system scheme, in which the lead pass through a hole and is subject to change its section while dissipating energy is displayed.

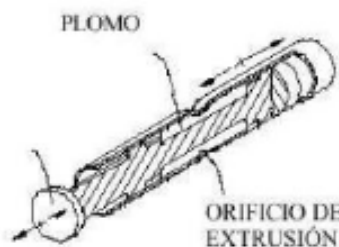


Figure 6. Dissipator by lead extrusion (Cahis, 2000)

Its hysteric response is very stable under several displacement cycles. A 200 kN model, able to resist displacement up to 10 mm and start dissipating from 0.05 mm, keeps its hysteretic curve without any appreciable modifications after 144000 cycles with an amplitude of +/- 4mm (Cahis 2000, as cited in Chambilla, 2015).

5.4. SLB Connections

5.4.1. The conception of the idea

The beginning of the idea of the SLB connections, which are energy dissipators based on metal plastification, started in the year 1989 during a personal conversation between the Dr Luis Bozzo and the distinguished Professor Popov in the University of California, Berkeley, who stated in reference to the popular structural system of eccentric steel frames that “steel is an excellent energy dissipator under shear forces”. Since normally concrete is associated to brittle failure under shear forces, the referred observation to the steel called particularly the attention of Dr Luis Bozzo. This observation refers to the dissipative capacity of metallic eccentric frames, thus, it is natural to think of joining passive control of structures with classical design through dissipative controlled zones. The SLB connections present high ductility, which is ideal for earthquake resistant structures, but with displacement of rigid systems, concentrating ductility demands in connections industrially manufactured. Experimental studies have shown that it is possible to design structures with level of forces of a flexible system but with displacement level of a rigid system, achieving one of the main aims of the

seismic resistant design. Because of the manufacturing process and easy replacement of the SLB connections, the idea of using these devices on uncoupled walls is introduced (Bozzo & Gaxiola, 2015).

Shear Link (SL) connections, which is how the device was called during its beginnings, develop hysteretic curves that are utterly uniform and described by low strength reduction. Uniform hysteretic curves means that the yielding must occurred before buckling of the thinner sections develops provoking a significant cutback of its capacity to dissipate energy (Nuzzo, et al., 2015).

5.4.2. First researches

The first research done is this topic was numerical and published in the article written by Foti (1998). In this first report, structural responses incorporating generic dissipators of energy were compared numerically determining its potential reduction of forces between flexible (without dissipators) and rigid systems (with dissipators).

Afterwards, Cahis, et al (1998) presented a SL dissipator to protect masonry walls from seismic events. The most important contribution explained in the prior is the application of the mechanizing process in order to avoid welding. This process allows to obtain eccentric braces which displayed that it was possible to design structures with seismic forces developed by flexible structures but with displacements developed by rigid structures.

As stated by Cahis, Torres and Bozzo (2000) from experimental and numerical studies is understood that masonry partitions add stiffness to frames and change its damping capacities. Usually, designers neglect their effect in the structural analysis since it is difficult to take advantage of their stiffness and strength; besides, masonry partitions cannot resist large deformations.

Limiting the drift is the most used solution to protect these non-structural elements. Another proposed solution is the uncoupling of the resistant structure from the masonry elements. However, using this technique it is not possible to take advantage of the stiffness and strength of the walls.

A different technique proposed by Yanev and Mc Niven (Cahis, et al., 2000) is to link the infill walls and resisting structural elements using designed metal springs.

Cahis, et al. (2000) proposes to replace the spring afore mentioned by a new SL dissipator fabricated without welding in areas where yielding takes place, and making possible to design very small web thickness devices to protect walls and, at the same time, to take advantage of the well-established properties of passive control systems..

5.4.3. Experimental tests and numerical models.

Several experimental tests and their corresponding numerical models have been executed to understand more about the energy dissipating behaviour of the SLB connections, the most relevant are described in the following paragraphs.

Cahis, et al. (2000) presented a study about the experimental behaviour on a Thick Flanged SL dissipator which has an I-shaped cross section with thick and narrow flanges. The test consisted of four specimens (A, B, C, and D) using a horizontal cycling loading machine at ISMES (International School for Materials for Energy and Sustainability). The test was executed in quasi-static conditions with an increment of one inch of amplitude per cycle. The four specimens develop similar hysteretic curves avoiding buckling. Once damage has been displayed, there was an extra amount of energy being dissipated. This effect happened due to flanges and stiffeners capability to stand damage since their thick and narrow geometry. Figure 8(a) shows the state of the SL-device before and after web damage has occurred.

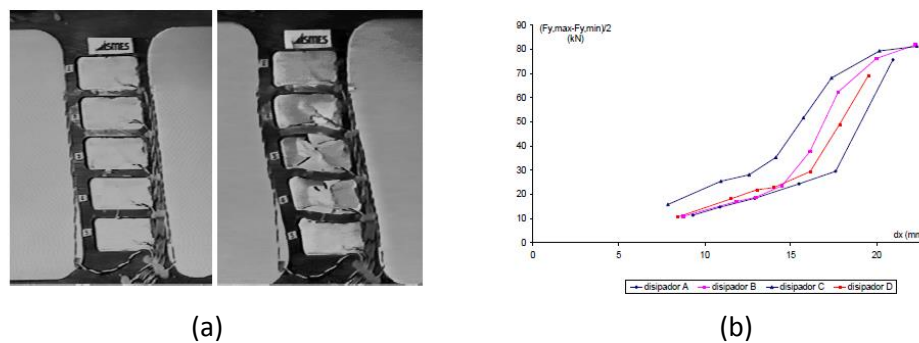


Figure 7. (a) A-device before and after web damage occurs. (b) Maximum cycle vertical force (semi-sum) versus displacement in the four devices. (Cahis, et al., 2000)

The results obtained are presented in table 1, the most important parameter is the transition radius (ϕ) which displays the efficiency of the dissipator as compared with perfect elasto-plastic behaviour. It has been seen that when large displacements are used and vertical displacements are repressed, axial force should arise. Therefore, when web damage starts appearing, vertical response evolution declines and vertical reactions get high levels. Figure 7(b) displays the Force – displacement evolution for the peak vertical reactions gotten for each cycle at its maximum response measured by displacements.

Table 1. Experimental values for the considered main parameters (Cahis, et al., 2000)

| | $F_{x,y}$ (kN) | $D_{x,y}$ (mm) | F_m (kN) | $F_{m,0}$ (kN) | E (kJ) | d_T (m) | $\Phi_{m,0}$ | ϕ | Y_T |
|---|-------------------|-------------------|---------------|-------------------|-------------|--------------|--------------|--------|-------|
| A | - | - | 43.46 | 37.95 | 21.28 | 0.731 | 1.965 | 0.768 | 5.375 |
| B | - | - | 42.35 | 37.94 | 15.16 | 0.517 | 1.964 | 0.767 | 3.801 |
| C | 14.45 | 0.538 | 35.88 | 30.83 | 10.43 | 0.426 | 2.01 | 0.791 | 3.132 |
| D | - | - | 40.28 | 34.98 | 15.62 | 0.563 | 1.811 | 0.793 | 4.140 |

Hurtado & Bozzo (2008) studied the behaviour of SL dissipators based on the eccentric braces structural system since its geometry displays a well stiffened wide-flange section. In order to define the most efficient geometry of the SL connection, four basic preliminary devices were tested at ISMES (International School for Materials for Energy and Sustainability). The software ANSYS was utilized to perform plastic nonlinear analyses. The steel structural constitutive models applied was the isotropic hardening.

Table 2. Selection criteria for the dimensions of the dissipators (Hurtado & Bozzo, 2008)

| Selection Criterion | Disip1SL30_2 | Disip2SL30_2 | Disip3SL30_2 | Disip4SL30_2 |
|--|--------------|--------------|--------------|--------------|
| 1. Milled area (cm ²) | 500 | 475 | 450 | 250 |
| 2. Number of windows | 2 | 4 | 6 | 4 |
| 3. Max. horizontal reactions (kN) | 154.54 | 160.392 | 167.015 | 229.296 |
| 4. Max. vertical reactions (kN) | 13.064 | 13.835 | 14.596 | 15.152 |
| 5. Maximum strain | 0.1437 | 0.1470 | 0.1515 | 0.2902 |
| 6. Maximum shear strain | 0.1651 | 0.1687 | 0.1749 | 0.3304 |
| 7. Post-yielding slope | 34.986 | 37.2273 | 41.3124 | 64.6584 |
| 8. Initial stiffness (kN/cm) | 2300.35 | 2422.05 | 2552.15 | 3238.60 |
| 9. Dissipated energy (kN.cm) | 237 | 248 | 260 | 346 |
| 10. Yielding force (kN) | 85.984 | 87.425 | 85.853 | 102.016 |
| 11. Yielding displacement (mm) | 0.405 | 0.40 | 0.354 | 0.315 |
| 12. Web buckling displ.(mm) | 4.98 | 8.95 | 17.87 | 14.2 |
| 13. Von Mises stresses (kN/cm ²) | 41.342 | 41.661 | 42.491 | 50.069 |
| 14. Max. shear stress (kN/cm ²) | 23.742 | 24.051 | 24.530 | 28.445 |

Table 2 displays the results obtained. Devices Disip1SL30_2 and Disip2_SL30_2 are disregarded due to web buckling. The device Disip4SL30_2 displays higher stiffness and better energy dissipating capabilities than Disip3SL30_2; nonetheless, it requires to use materials with higher ductility levels. Therefore, the device Disip3SL30_2 is selected to study its hysteretic behaviour.

5.4.4. Mathematical models

Nuzzo, et al. (2015) presented a mathematical model to evaluate the response of Shear Links acting on braces which assumes that the SL height and base are established; therefore, the only unknown variables are the thickness of the called “windows” (thinner sections), e , and the thickness of the other section of the shear link, t . Thus, it provides a mathematical approach of two equations and two unknown variables. The diagonal stiffness, k_d , is represented by

$$k_d = \frac{A_d * E}{L}, \quad (1)$$

the stiffness of each window can be represented by

$$k_w = \frac{G * A}{h}, \quad (2)$$

the stiffness of the thicker section of the SL device can be represent by:

$$k_r = \frac{48 * E * I}{h^3}, \quad (3)$$

the afore mentioned stiffness can be represented by the schematic diagram in figure 8.

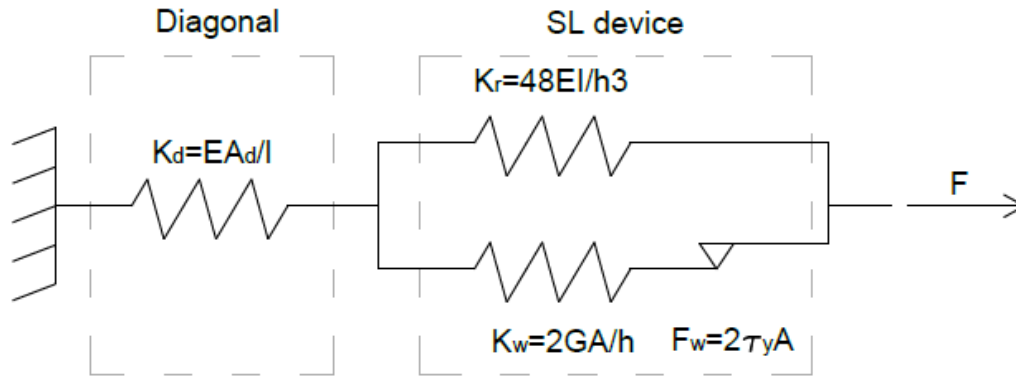


Figure 8. Analytical scheme of the composed system diagonal + SL device (Nuzzo, et al., 2015)

The applied force in parallel, F , to the system is obtained by adding the forces in each element; besides, all elements share the same displacement as shown by

$$F = F_w + F_r = k_w * x_w + k_r * x_r = (k_w + k_r) * x, \quad (4)$$

$$x_w = x_r = x, \quad (5)$$

the stiffness equation for the SL device before yielding can be represented by,

$$k_{diss1} = \frac{F}{x} = \frac{(k_w + k_r) * x}{x} = k_w + k_r, \quad (6)$$

after yielding, the previous equation becomes

$$k_{diss2} = k_r. \quad (7)$$

Figure 9 displays the force-displacement relationship of each element separately and of the whole system. Hence, if the applied force is less than the yielding force, the equivalent stiffness is the sum of displacements of each level; however, if the applied force is larger than the yielding force, just the SL device stiffness represents the whole stiffness of the system.

Besides, they explained that this SL device is suitable to be used as a link between the flexible frame and a conventional steel bracing system; however, it could be conveniently used as link between flexible frames and masonry walls. In order to demonstrate the capabilities of the SL connections, the geometry of the structure to be tested was chosen to be comfortable as cheap for residential purposes. It allowed to estimate the structural behaviour of the SL

connections and propose analytical models which through the use of numerical simulations can be proposed a method to analyse the structure performance in commercial softwares. Finally, FEMA procedures were adopted to estimate the effective damping provided by the SL device which can be used for implementing easier and faster linear analysis.

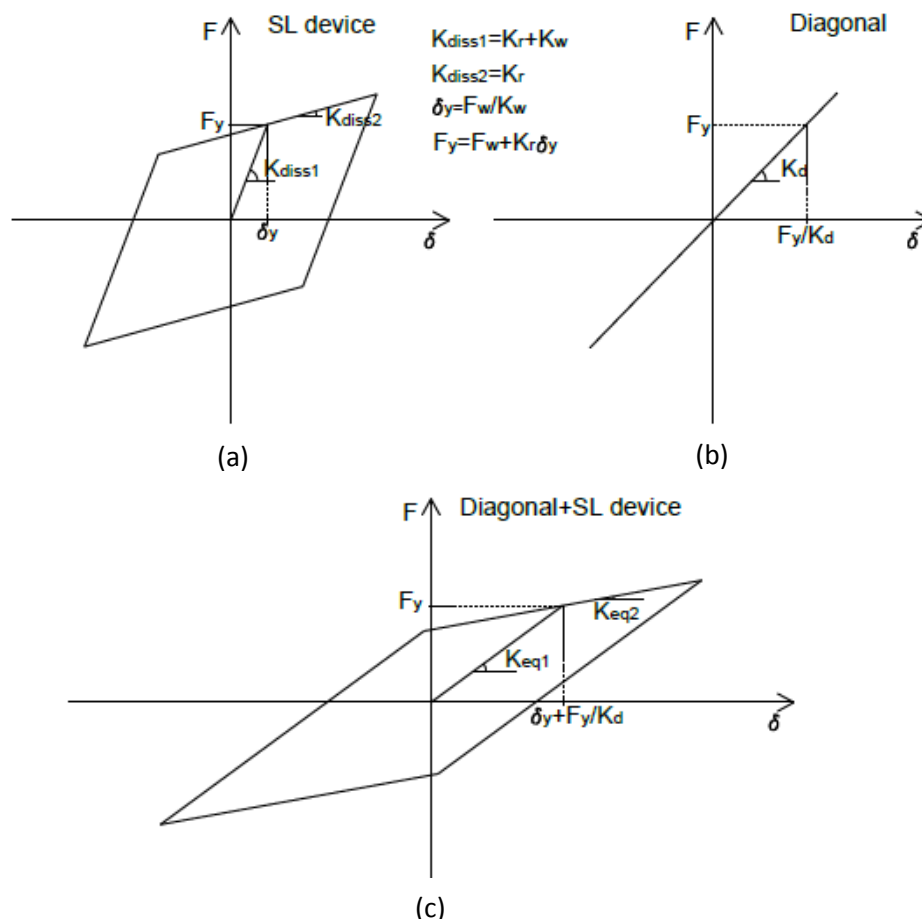


Figure 9. (a) Force-displacement diagram of the SL device. (b) Force-displacement diagram of the diagonal structure. (c) Force-displacement diagram of the Diagonal + SL device (Nuzzo, et al., 2015).

5.4.5. Geometry and Manufacturing process

Hurtado & Bozzo (2008) described that the shape of a SL connection is a well strengthened wide-flange area. The manufacturing process implies that the device is obtained from a plane shape by a milling process. This manufacturing process proposed by Cahis (1998) makes possible to use very thin dissipative areas which allows the SL dissipator to perform a double-mode work. First, a shear mode is displayed when the energy is dissipated by shear stresses in the web. Next, a flexural mode takes place due to energy being dissipated by the stiffeners preceded by web degradation.

The milling process allows to design an assortment of SL devices with different mechanical characteristics avoiding brittle behaviour since welding manufacturing processes

are not utilized. One of the main characteristics of the milling process is that it allows manufacturing in large scale which permits to have a better quality control procedure.

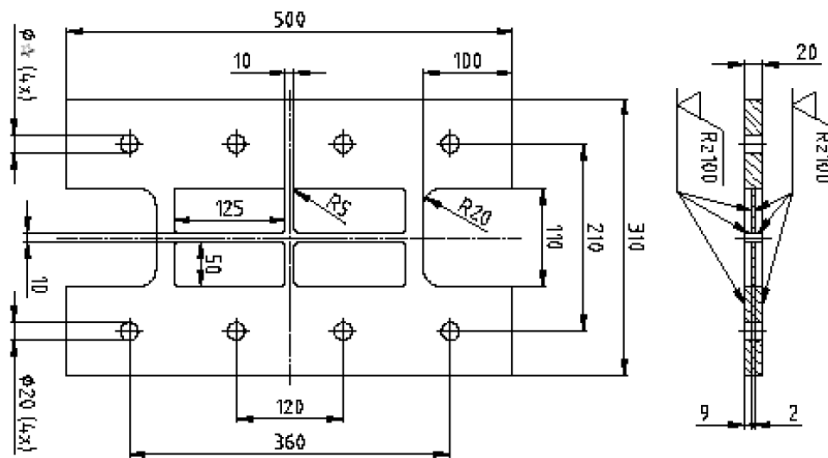


Figure 10. Dimensions for the Disip4SL30_2 device (Hurtado & Bozzo, 2008)

5.4.6. Design tables

Hurtado (2008) introduced a summation of the design parameters that affect the most the behaviour of the Shear Links. The devices are labelled as SLX_Y where X indicates the total width and Y indicates the web thickness. It is provided a wide variety to choose as displayed in table 3; the parameter X varies from intervals of 50 to 500 mm, and the parameter Y could be 2, 3, 4 or 5. It is proposed 32 type of devices which behave similarly resulting in a broad selection as requested by design.

6. Test setup

6.1. SLB connections

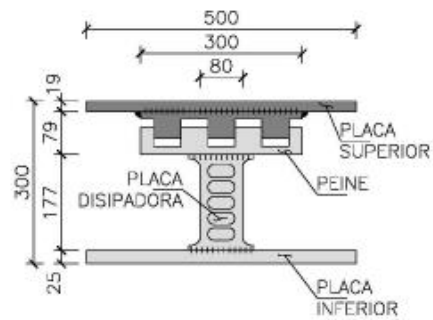
SLB connections of different capacities were used (figure 11). The first is named “type 1”, which has a lateral design strength of 125 KN each. The second one is named “type 2” which has a lateral design strength of 250 KN each. Their dimensions are shown in the figure 11(a) and 11(c). The main characteristic of the SLB device tested is the upper connection called “comb”, these connections transfer only displacements avoiding completely the transmission of axial load over the devices. The material of the steel connections is structural steel ASTM A36, with a nominal strength of $F_y = 250$ MPa.

To link the SLB connections with the structure, high strength screws were used with diameters of 19 mm and 25 mm. The screws of 19 mm were placed horizontally to connect the concrete elements. The screws of 25 mm were placed vertically to connect the upper and lower plates of the SLB connections to the connecting plates of the concrete elements. In total, in each SLB connection, 32 screws were used, 16 on the top and 16 on the bottom. In one of the connecting plates with the shear wall, it was not possible to locate one of the screws since a

steel bar was found while boring; therefore, it was decided to maintain it although a screw was not connected. It generated a premature failure of the connection; although, the dissipators still had capacity to dissipate energy. Besides, the screws were placed without mortar which triggered an anticipated deterioration under cyclic loading.

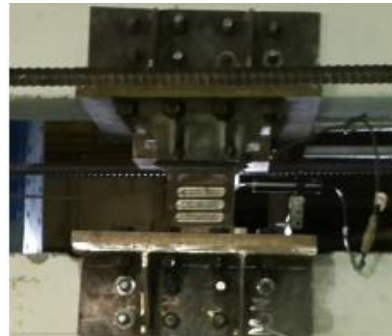
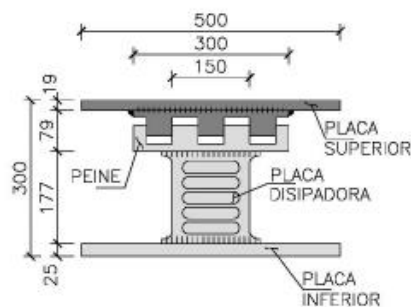
Table 3. The most relevant design parameters for the devices (Hurtado & Bozzo, 2008)

| Device | e | K ₁ (kN/cm) | K ₂ (kN/cm) | d _y (mm) | f _y (kN) | D _y (mm) | F _y (kN) | F _{max} (kN) | D _a (mm) | E _d (kN-cm) |
|--------|---|---------------------------|---------------------------|------------------------|------------------------|------------------------|------------------------|--------------------------|------------------------|---------------------------|
| SL5_2 | 2 | 546.1 | 14.4 | 0.250 | 13.65 | 0.463 | 25.27 | 47.32 | 39.93 | 54 |
| SL5_3 | 3 | 663.5 | 13.4 | 0.321 | 21.3 | 0.549 | 36.40 | 56.59 | 89.87 | 69 |
| SL5_4 | 4 | 763.8 | 11.8 | 0.357 | 27.27 | 0.628 | 47.96 | 65.26 | 159.83 | 84 |
| SL5_5 | 5 | 834.3 | 8.8 | 0.357 | 29.78 | 0.716 | 59.76 | 72.93 | 249.81 | 97 |
| SL10_2 | 2 | 1273.8 | 22.1 | 0.250 | 31.85 | 0.437 | 55.68 | 89.56 | 29.81 | 109 |
| SL10_3 | 3 | 1644.4 | 21.6 | 0.277 | 45.55 | 0.491 | 80.67 | 113.62 | 67.10 | 146 |
| SL10_4 | 4 | 1979.1 | 20.1 | 0.304 | 60.16 | 0.540 | 106.86 | 136.91 | 119.35 | 182 |
| SL10_5 | 5 | 2216.7 | 17.4 | 0.331 | 73.26 | 0.600 | 133.00 | 159.27 | 186.45 | 216 |
| SL15_2 | 2 | 2285.9 | 22.4 | 0.250 | 57.15 | 0.567 | 129.60 | 163.04 | 20.29 | 216 |
| SL15_3 | 3 | 2929.6 | 23.3 | 0.268 | 78.51 | 0.565 | 165.55 | 200.32 | 45.66 | 271 |
| SL15_4 | 4 | 3493.5 | 22.9 | 0.286 | 99.91 | 0.573 | 200.20 | 236.30 | 81.18 | 325 |
| SL15_5 | 5 | 3856.1 | 22.3 | 0.321 | 123.78 | 0.618 | 238.33 | 271.48 | 126.85 | 377 |
| SL20_2 | 2 | 2971.2 | 24.1 | 0.250 | 74.28 | 0.536 | 159.18 | 195.36 | 15.96 | 262 |
| SL20_3 | 3 | 3980.0 | 24.9 | 0.268 | 106.66 | 0.527 | 209.68 | 247.72 | 35.92 | 339 |
| SL20_4 | 4 | 4719.3 | 25.8 | 0.286 | 134.97 | 0.553 | 261.00 | 298.88 | 63.85 | 414 |
| SL20_5 | 5 | 5262.7 | 24.0 | 0.321 | 168.83 | 0.596 | 313.46 | 349.12 | 99.77 | 489 |
| SL25_2 | 2 | 3660.6 | 24.3 | 0.250 | 91.51 | 0.514 | 188.18 | 224.74 | 14.44 | 305 |
| SL25_3 | 3 | 4859.0 | 25.2 | 0.268 | 130.22 | 0.524 | 254.52 | 292.09 | 32.50 | 404 |
| SL25_4 | 4 | 5921.3 | 24.7 | 0.286 | 169.35 | 0.544 | 321.82 | 358.05 | 57.79 | 501 |
| SL25_5 | 5 | 6613.5 | 24.5 | 0.321 | 212.29 | 0.588 | 389.20 | 423.17 | 90.30 | 597 |
| SL30_2 | 2 | 4353.6 | 24.5 | 0.250 | 108.84 | 0.497 | 216.56 | 253.78 | 13.75 | 348 |
| SL30_3 | 3 | 5791.0 | 25.5 | 0.268 | 155.20 | 0.513 | 297.22 | 336.02 | 30.93 | 468 |
| SL30_4 | 4 | 7129.9 | 25.4 | 0.286 | 203.91 | 0.531 | 378.46 | 416.81 | 54.99 | 587 |
| SL30_5 | 5 | 7981.8 | 25.2 | 0.321 | 256.21 | 0.575 | 459.17 | 496.73 | 85.92 | 704 |
| SL40_2 | 2 | 5820.4 | 30.9 | 0.250 | 145.51 | 0.490 | 285.12 | 331.02 | 14.02 | 455 |
| SL40_3 | 3 | 7778.5 | 32.0 | 0.268 | 208.46 | 0.507 | 394.44 | 442.74 | 31.55 | 619 |
| SL40_4 | 4 | 9621.2 | 33.1 | 0.286 | 275.17 | 0.523 | 503.33 | 553.98 | 66.90 | 781 |
| SL40_5 | 5 | 10777.4 | 31.8 | 0.321 | 345.95 | 0.570 | 614.29 | 662.15 | 104.53 | 941 |
| SL50_2 | 2 | 7223.6 | 32.9 | 0.250 | 180.59 | 0.473 | 342.00 | 391.08 | 13.40 | 542 |
| SL50_3 | 3 | 9703.1 | 35.9 | 0.268 | 260.04 | 0.495 | 480.00 | 533.58 | 30.16 | 749 |
| SL50_4 | 4 | 12109.3 | 32.7 | 0.286 | 346.33 | 0.514 | 622.22 | 671.76 | 53.62 | 954 |
| SL50_5 | 5 | 13566.7 | 31.0 | 0.321 | 435.49 | 0.563 | 764.00 | 810.65 | 83.79 | 1160 |



(a)

(b)



(c)

(d)

Figure 11. (a) Dimensions of SLB connection type 1. (b) SLB connection type 1. (c) Dimensions of SLB connection type 2. (d) SLB connection type 2 (Instituto de Ingenieria UNAM, 2017).

6.2. Concrete Frame

The reinforced concrete frame is composed of prefabricated elements, which includes: two columns of 30 x 30 cm, a beam of 22 x 40 cm and a shear wall of 15 cm of thickness. The beam is linked to the shear wall through rigid bolted connections. The dimensions and steel reinforcement are shown in figure 13. It is important to emphasize that the concrete frame and the shear wall are not linked physically. The link between them are the SLB connections. Thus, when there are no SLB connections, the elements work separately. The SLB connections link the shear wall and concrete frame to create a frame – wall – SLB connections system. In figure 12, it is also seen that the shear wall and columns were set over rigid foundations; the foundations were anchors applying a tension force of 200 kN which allowed to emulate fixed supports.



Figure 12. Reinforced concrete frame used in the test (Instituto de Ingenieria UNAM, 2017)

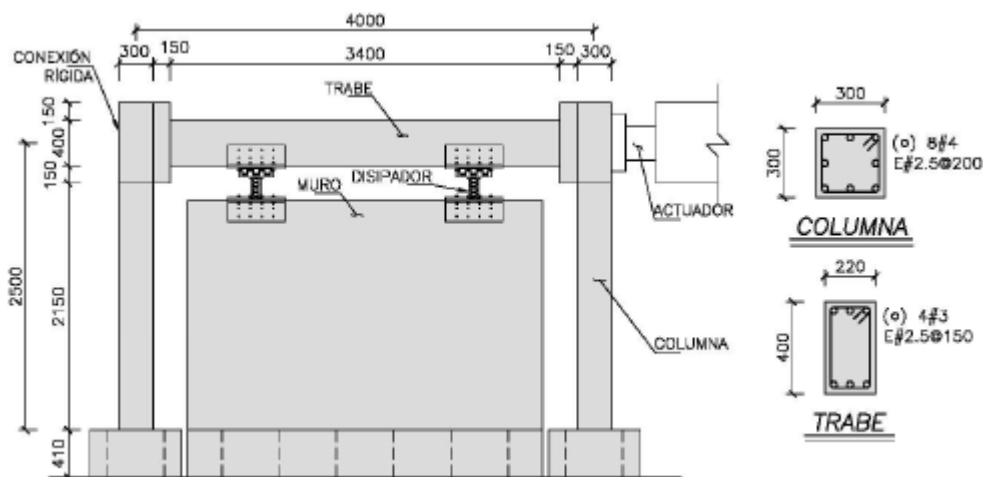


Figure 13. Dimensions (mm) of the reinforced concrete frame. (Instituto de Ingenieria UNAM, 2017)

6.3. Instrumentation

To measure the displacement of the frame, generated by the actuator, two types of instruments were used. The first consisted of displacement transducers type CDP of the brand Tokyo Sokki Kenkyujo, with a measurement capacity of ± 25 mm. the second was located as alternative and consisted of a high resolution camera type Optotrak Certus HD and Leds to follow the displacement.

Figure 14 shows the first instrumentation type (with CDPs). It is possible to see that the most relevant instrument was labelled as “1”, since it allowed to measure the imposed displacements directly. Hysteresis curves of the model were obtained through plotting the displacement variation of the CDP 1 as a function load imposed by the hydraulic actuator.

Figure 15 shows the second instrumentation type. It is shown that many points in the frame were measured using Leds. In this figure it is seen that it is possible to obtain relative displacements in three directions among each point (or Led).

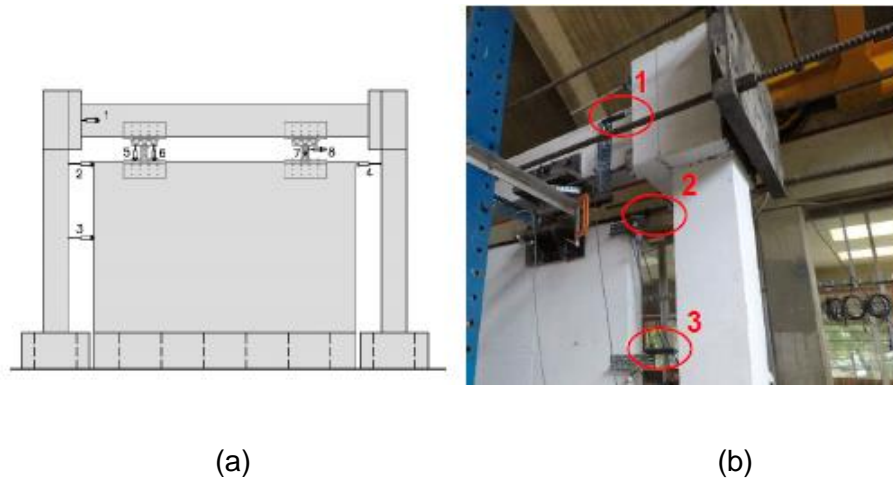


Figure 14. (a) Instruments location. (b) CDPs location. (Instituto de Ingenieria UNAM, 2017)

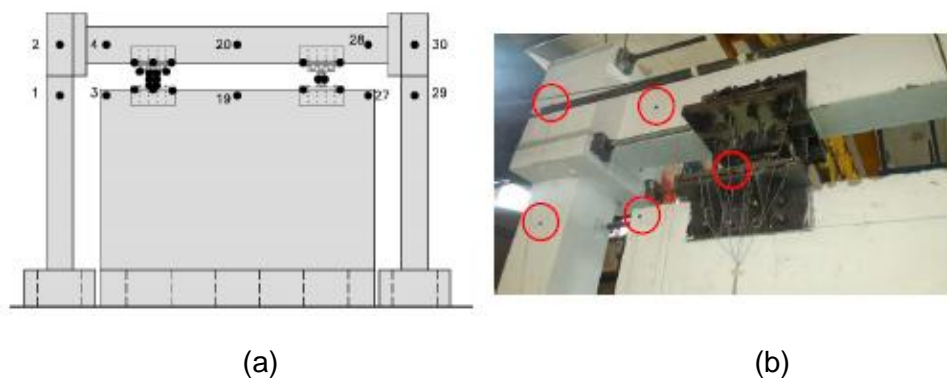


Figure 15. (a) Leds location. (b) Leds in the test setup. (Instituto de Ingenieria UNAM, 2017)

6.4. Loading pattern

Figure 16 shows the loading pattern used. It consists of a history of displacements applied statically, with an actuator MTS with a capacity of ± 1000 KN and a maximum displacement of 200 mm. All the tests were controlled by displacements. Moreover, it is seen that the displacements were applied from 1 to 18 mm; and four loading cycles per each displacement level. At the end of the tests with a SLB connection type 1, 20 cycles of 18 mm were applied in order to fatigue the SLB connection. While using the connection type 2, some additional cycles were applied with higher deformation levels. Those are shown in the results section since this was not contemplated in the initial loading program.

It is important to mention that all displacements were controlled using the hydraulic actuator dial. This considers small differences with the obtained measurements using

instrumentation based on displacement transducers due to deformation in the actuator and reaction wall.

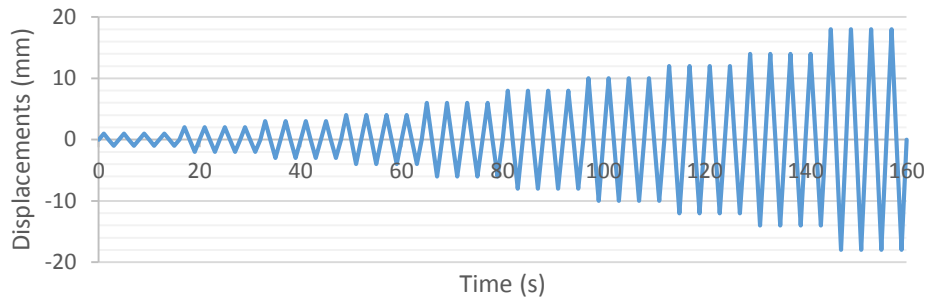


Figure 16. Pattern of applied displacements.

6.5. Experimental results

6.5.1. Hysteresis curves

Figures 17 to 19 show the hysteresis curves and envelopes obtained in each of the test: the frame without SLB connections, the frame linked by SLB connections type 1 and the frame linked by SLB connections type 2. In order to compare, all figures are using the same scale. The following observations can be made:

6.5.1.1. Frame without SLB connections under monotonic cyclic load

Using the imposed displacements, the reinforced concrete frame shown a quasi-elastic linear behaviour (figure 17). The total lateral force applied, to achieve maximum positive displacement of 14 mm, was 72 kN; meanwhile; for achieving the maximum negative displacement of 14.4 mm, it was 63.4 kN.

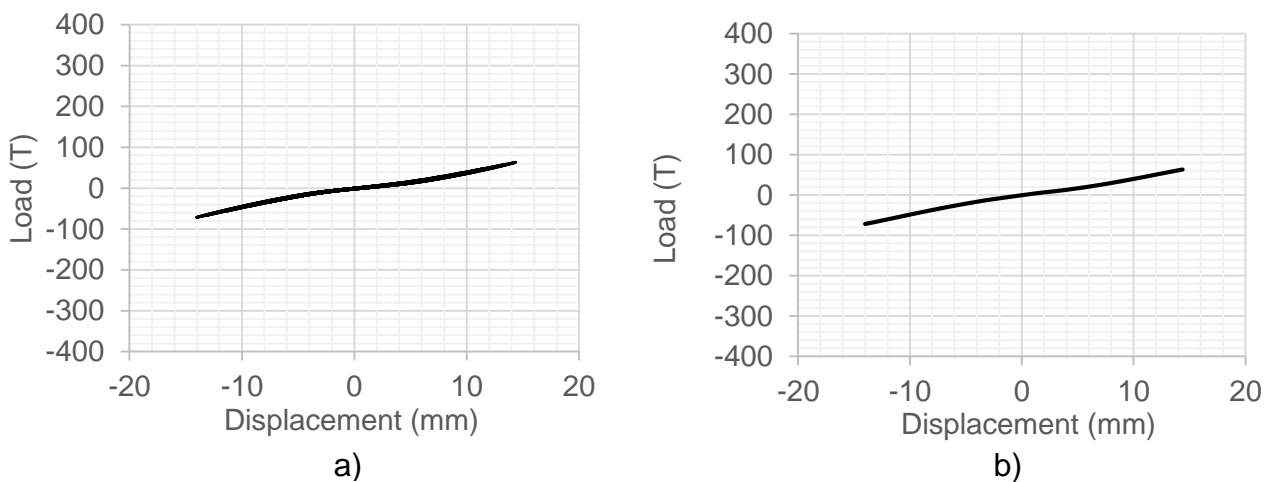


Figure 17. (a) Hysteresis curve – Frame without SLB connections. (b) Hysteresis curve envelop - Frame without SLB connections. (Instituto de Ingenieria UNAM, 2017).

6.5.1.2. Frame with SLB connections type 1 under monotonic cyclic load

Using the SLB connections type 1 (figure 18), the structural system behaved non linearly, with a yielding load and displacement close to 100 kN and 2mm respectively forward and backwards. After yielding, with a positive slope, the system reached a lateral load of 234 kN with a maximum positive displacement of 15 mm, and 236 kN with a maximum negative displacement of 14.2 mm.

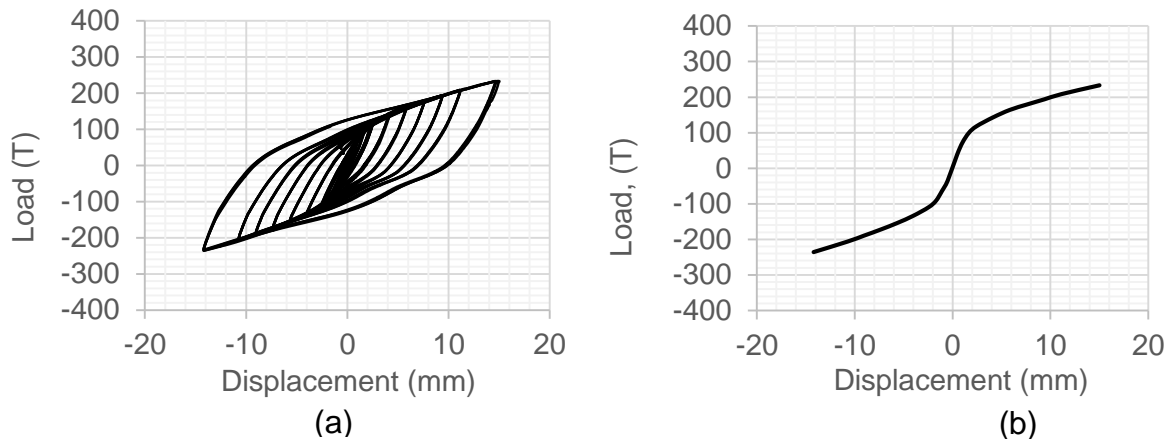


Figure 18. (a) Hysteresis curve – Frame with SLB connections type 1. (b) Hysteresis curve envelop – Frame with SLB connections type 1 (Instituto de Ingenieria UNAM, 2017).

6.5.1.3. Frame with SLB connections type 2 under monotonic cyclic load

Using SLB connections type 2, the structural system also behaved nonlinearly (figure 19). However, a thinning in the hysteresis curves has been observed. It was produced by displacement of the connecting plates of the SLB connections and shear wall. The yielding lateral load of the system was 130 kN with a displacement of 2 mm. After yielding, it is seen the positive slope in the curves reaching a maximum lateral load of 316 kN with a maximum positive displacement of 13.3 mm, and a maximum negative displacement of 12.7 mm with a lateral load of 325 kN.

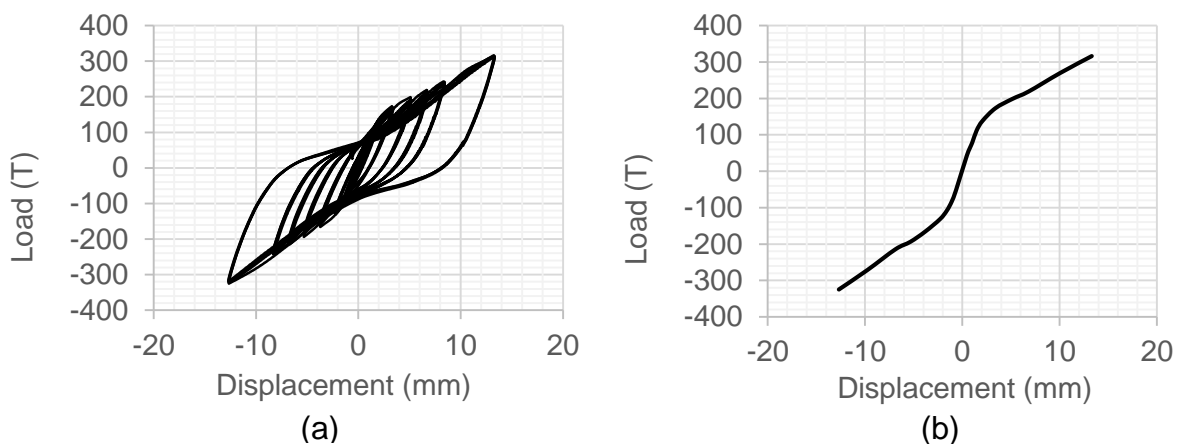


Figure 19. (a) Hysteresis curve – Frame with SLB connections type 1. (b) Hysteresis curve envelop – Frame with SLB connections type 1 (Instituto de Ingenieria UNAM,

7. FEA modelling

In order to simulate the behaviour of the afore mentioned tests, the finite element analysis software ABAQUS CAE was used to get requested results through modelling, analysis, assembling, and visualization of structural components.

Only the frame without SLB connections and the frame with SLB connections Type 1 are modelled in this report since the frame with SLB connections Type 2 displayed an unexpected behaviour due to excessive displacements of the connecting plates according to the recorded video of the test (Bozzo, 2017).

7.1. Mesh discretization

In order to analyse the FEA model using ABAQUS CAE, the concrete elements of the test such as beam, columns, steel plates, and joints are idealized using homogeneous material properties and modelled with eight-node solid elements, which are named C3D8R. C3D8R elements are selected since they output proper results for nonlinear static and dynamic analyses (Ahmed, 2014). The longitudinal reinforcement bars are modelled as truss embedded in the concrete elements, which according to ABAQUS are named T3D2. T3D2 stands for 2-node linear 3-D truss elements. The SLB connections as well as welding are model as C3D10 which stands for a 10-node quadratic tetrahedron, this type of element was chosen due to its complex geometry. To develop the model mesh and obtain results in a moderate amount of time, a course mesh is used in elements which do not influence the overall behaviour of the structure under cyclic loads like the beam and joints and fine mesh is used in elements like columns and SLB connections since their stress distribution influences greatly the behaviour of all structure. The solid element model consists of 7931 nodes. Sensitivity meshing issues are presented in Appendix B.

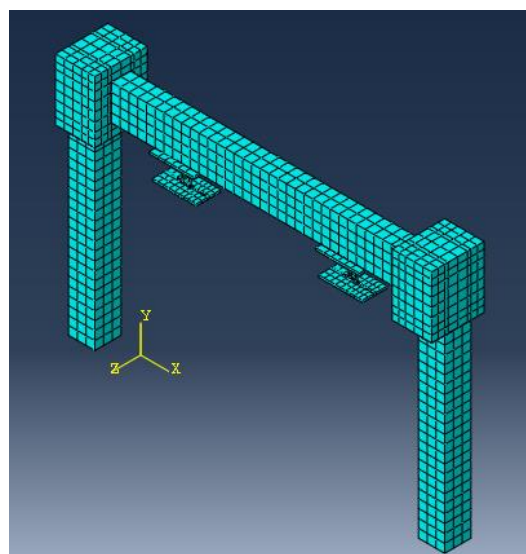


Figure 20. Mesh configuration of FE model of the test

7.2. Material properties

All material properties are specified according to the information obtained from the test; however, high-quality material data were not available; therefore, many parameters are assumed according to ABAQUS CAE user manual and other sources. The validation process depends greatly of the accuracy of the material data used, thus, elasticity and plasticity models are employed to depict mechanical constitutive models for all the materials used.

7.2.1. Constitutive model of reinforcing bar steel

Usually, the behaviour of the steel reinforcing bars is linear elastic at low strain demands. However, under high strain demands, it behaves inelastically, which implies plastic performance after reaching its yielding point. Before reaching its yielding point, deformation can be fully recovered if load is removed. Nonetheless, exceeding yield stresses will develop permanent deformations diminishing the stiffness of the section. (Ahmed, 2014)

The yield strengths for longitudinal steel bars was considered as 420 MPa with Young's modulus of elasticity, $E_s = 200$ GPa and Poisson's ratio, $\mu = 0.3$.

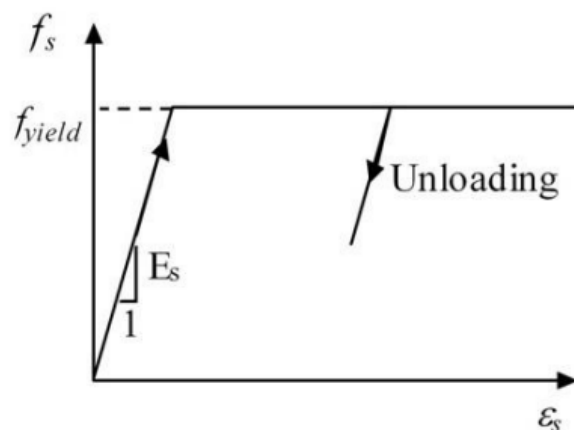


Figure 21. Elastic-perfectly plastic behaviour of steel bars (Broujerdian, 2016)

7.2.2. Constitutive model of SLB connection steel

Aguiar (2002) states that there are different constitutive models to define the behaviour of structural steel, the ones that are more recognized are the elastoplastic model, trilinear model and the complete curve model. The first is widely used in design due to its ease to use and provision of safety to the designer; however, it is not suitable for analysis since it ignores steel strength for large deformation over yielding limit. The trilinear model, is an accurate idealization and is used when a structural element is subject to large deformation, and if a high level of accuracy is required, the complete curve model will be the most suitable. In this research, the trilinear model is being used, since the load pattern makes the structural steel in the SLB connections yield at minimum displacements and most of its behaviour displays plastic deformations.

The material used is a structural steel ASTM A36 with a nominal strength of $F_y = 250$ N/mm², the constitutive model used is trilinear (The Materials Information Society, 2002) as shown in Figure 22.

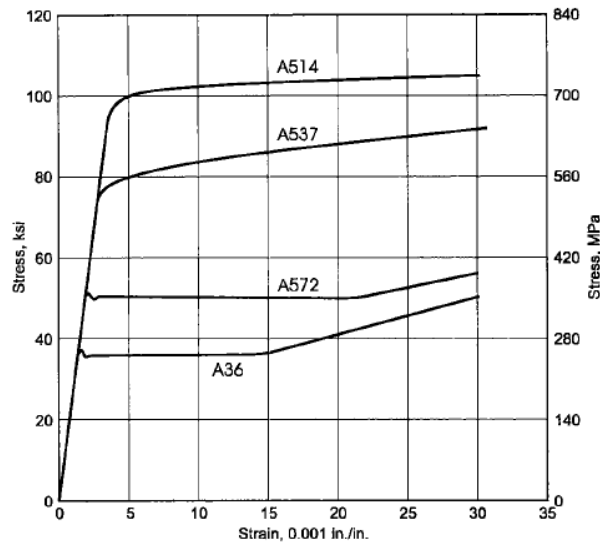


Figure 22. Structural steel A36 stress - strain curve (The Materials Information Society, 2002)

ASTM A36 steel plate is the most widely used hot-rolled steel product. As a kind of carbon structural steel product, its relative products are round rod steel, angle bar, and steel sections such as I-Beams, H-beams, angles, and channels. Hot rolled ASTM A36 has rough surface on the final product, and is versatile for further processing like machining (Agico Group, 2018).

7.2.3. Constitutive model of reinforced concrete

Linear at elastic and nonlinear damaged plasticity model for inelastic states of concrete are assumed because of low deformability of concrete in both states. The concrete isotropic damage plasticity model is designed for its cyclic loading conditions. Degradation of the elastic stiffness induced by the plastic straining both in tension and compression are taken into consideration in the material constitutive model.

- Concrete damage plasticity model

The material model used in this research is a plasticity based, damaged model for concrete. Damage plasticity describes the uniaxial tensile and compressive response of concrete as shown in Figure 23. First, the material develops a linearly elastic behaviour under uniaxial tension until the failure stress value σ_{t0} is reached. Further the failure stress state in concrete, stress-strain behaviour displays softening (Figure 23a). Under uniaxial compression,

the response is linear until reaching the initial yield σ_{c0} value. After reaching the ultimate stress σ_{cu} value in the plastic area, the concrete response is defined by the stress hardening behaviour; afterwards, strain softening behaviour is displayed (Figure 23b). (Dassault Systèmes Simulia Corp., 2010).

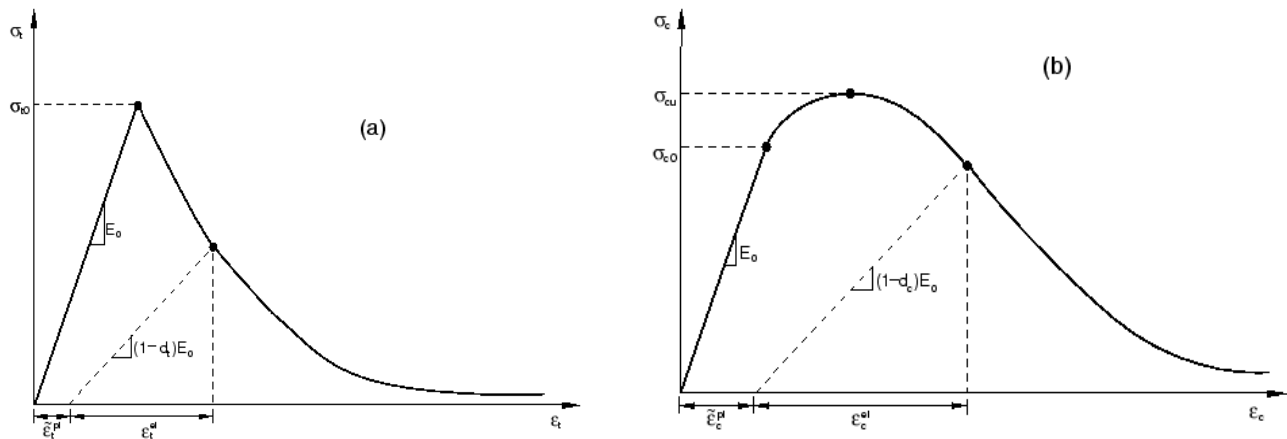


Figure 23. (a) Tension behaviour associated with tension stiffening. (b) Compressive behaviour associated with compression hardening (Dassault Systèmes Simulia Corp., 2010).

The concrete has been modelled using the constitutive model presented in Eurocode 2 for structural analysis. The Young’s Modulus of the concrete is 31926.07 N/mm², the Poisson’s Ratio value was assumed to be 0.2 and the crushing strength under compression is 34 N/mm² according to sample tests under uniaxial compression.

Besides, the plastic behaviour of the concrete is defined by the following parameters given in table 4.

Table 4. Concrete damage plasticity parameters (Dassault Systèmes Simulia Corp., 2010).

| Parameters | |
|----------------------------|--------|
| Dilation angle | 30° |
| Eccentricity | 0.1 |
| Fb0/fc0 | 1.16 |
| K | 0.6667 |
| Viscosity Parameter | 0.0001 |

7.3. Loading pattern

In order to reduce the computational processing time as much as possible while still obtaining accurate results, the loading pattern has been diminished as shown in Figure 24, this loading pattern is large enough to calibrate the numerical model until validation. Besides, the

displacement values have been varied since the whole structure has displayed lower displacement values due to adjustment between the surfaces of joints and actuator.

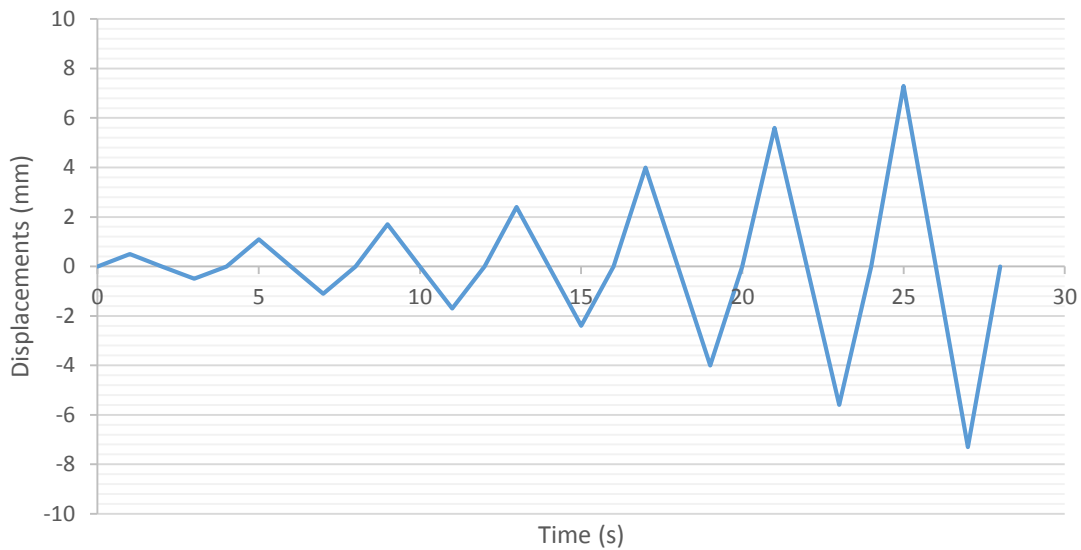


Figure 24. Adjusted loading pattern - numerical model

7.4. Boundary conditions

As the concrete columns and reaction wall were anchored using pretension forces, they behave as fixed supports. In the case of the reaction wall, it was considered to have minimum displacements according to its stiffness. Therefore, the reaction wall was modelled on ABAQUS CAE to get its behaviour which allowed to observe that the whole reaction wall behaved as infinitely rigid; however, according to the recorded video of the test (Bozzo, 2017), there were displacements and considerable rotations due to the lack of application of grout where clearances took place; therefore, modelling the reaction wall on ABAQUS CAE may not be the best solution. Hence, linear springs were used in order to simulate this unexpected state. In total 36 springs were used under the plates where the SLB connections were welded to the reaction wall.

Several iterations were executed in order to get the proper stiffness of the springs. Finally, the chosen springs to make the FEM model behave similarly than the test have a lineal stiffness as displayed in Table 5.

Table 5. Spring Stiffness

| Spring stiffness | |
|----------------------|-----------|
| X – stiffness | 350 N/mm |
| Z – stiffness | 1000 N/mm |

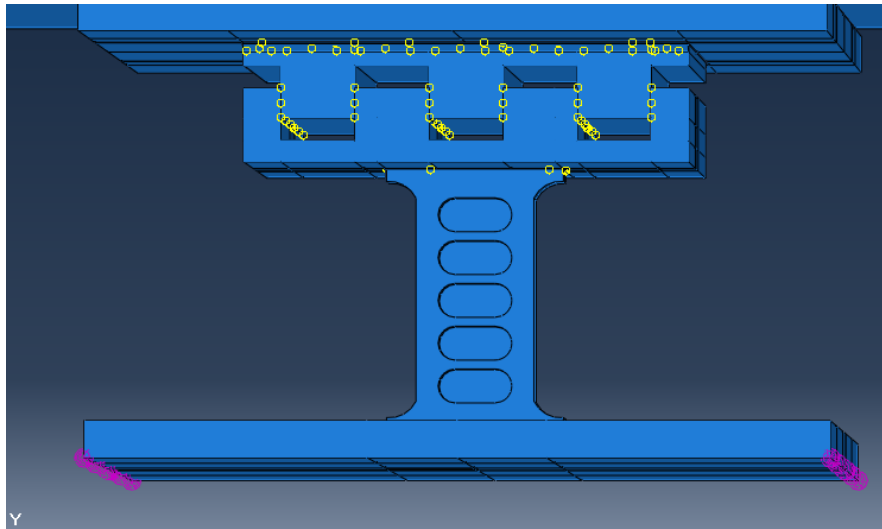


Figure 25. Springs position

7.5. Validation

It was necessary to model first the concrete frame without SLB connections in order to obtain its performance; afterwards, the uncoupled frame SLB connections type 1 was modelled until getting the right behaviour of the SLB connections.

7.5.1. Concrete frame without SLB connections

The first test executed was the “Uncoupled frame with SLB connections type 1”; during this test, the structure was subject to large displacements that provoked cracking in the concrete columns. Therefore, while testing the “Concrete frame without SLB connections”, it behaved displaying stiffness of a cracked section as shown in Figure 17 (a); on the other hand, the numerical model of the afore mentioned test displayed an uncracked followed by cracked behaviour as displayed in Figure 26.

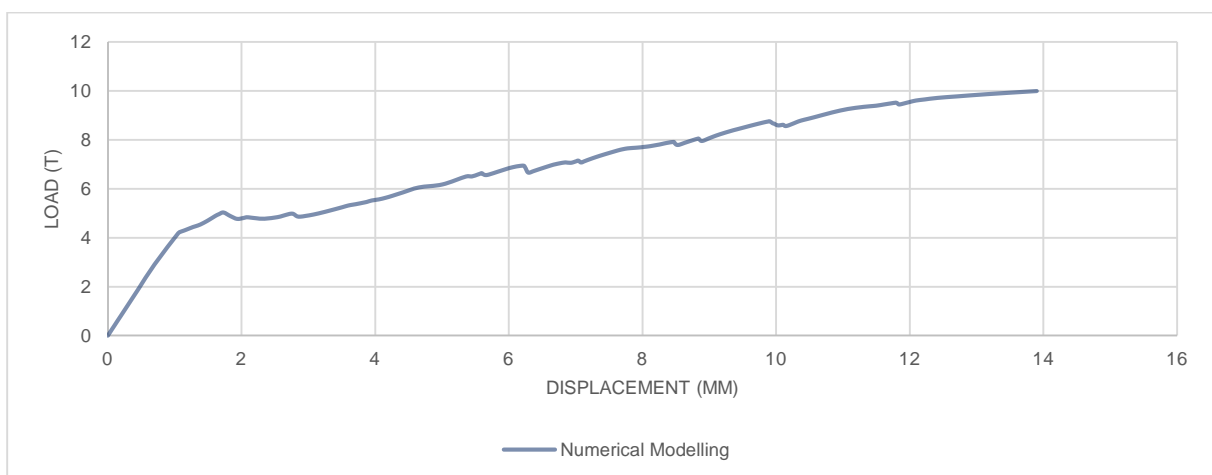


Figure 26. Load-Displacement relationship of "Concrete frame without SLB connections" (Experimental test)

Therefore, it has been decided to validate just the behaviour of the test once the concrete columns are completely cracked. Drawing a trend line in both, the results of the experimental test and the cracked behaviour of the numerical model, it can be seen in Figure 27 that both results display a highly similar stiffness of 0.51 T/mm allowing to understand that the numerical model simulates the structural behaviour of the test, this simulation was sufficient since during the test of the uncoupled frame with SLB connections type 1, the concrete columns did not present cracking at all at the beginning of the test.

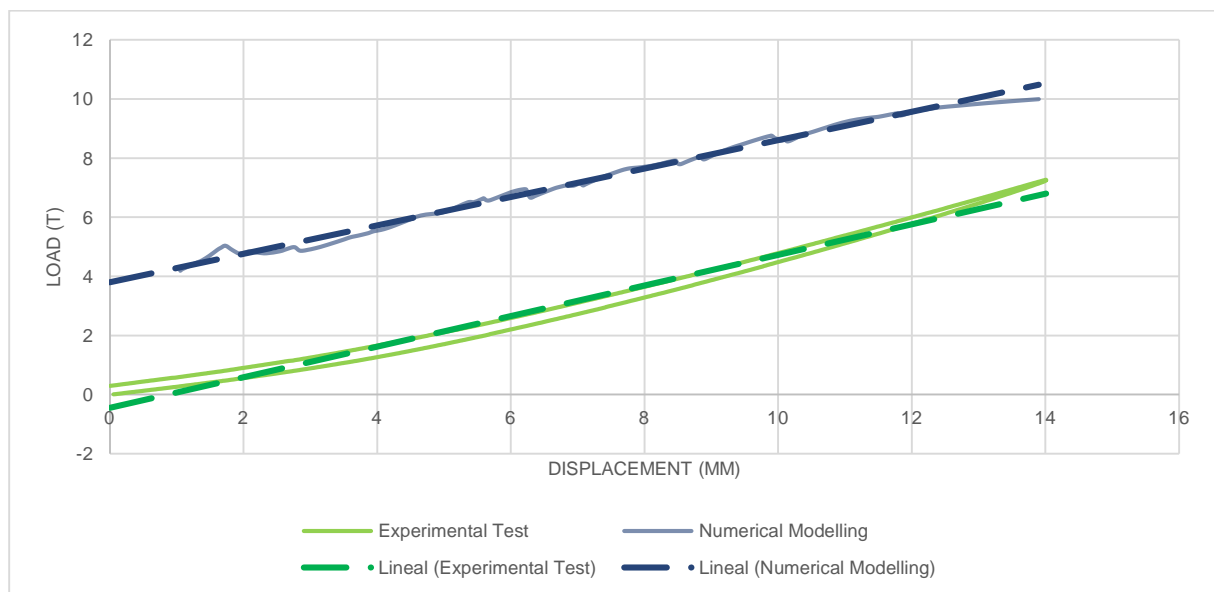


Figure 27. Load-Displacement relationship of "Concrete frame without SLB connections" (Experimental test – Numerical modelling)

7.5.2. Uncoupled frame with SLB connections type 1

Through several iterations to get the spring stiffness shown in table 5, it was possible to obtain a numerical model that displays a similar behaviour than the experimental test. The results of the numerical modelled shown well-shaped hysteretic curves with a minimal error of 1.14% about the highest value reached by the experimental test. Even though the highest values are similar to the results of the experimental tests, the overall shape of the hysteretic curves display yielding differently. This difference in shape may be produced by a nonlinear behaviour of the reaction wall which could be represented by the use of nonlinear springs.

As shown in Figure 29, the Von Mises stress distribution in the SLB connection type 1 is mainly distributed in the "windows" which are the thinner sections; however, the superior part of the frames also present high stress levels. Besides, the welding sections are subject to minimum levels of stress. On the other hand, sections like steel plates and steel type comb connection (located over the SLB connection) do not display any stress distribution since they behave as rigid bodies due to their compact geometry compared to the SLB connections.

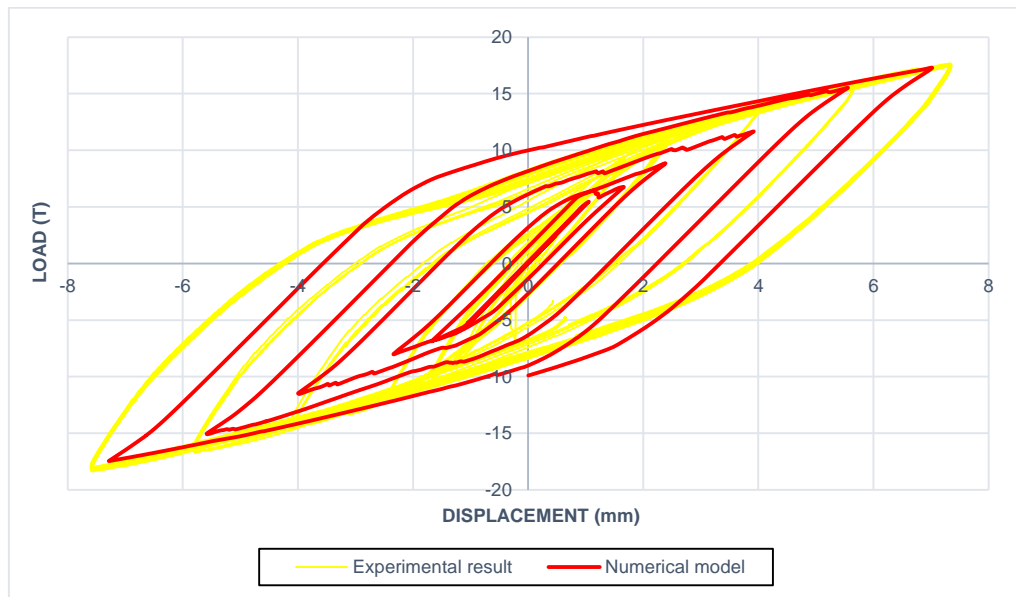


Figure 28. Force - Displacement relationship of SLB connections type 1.

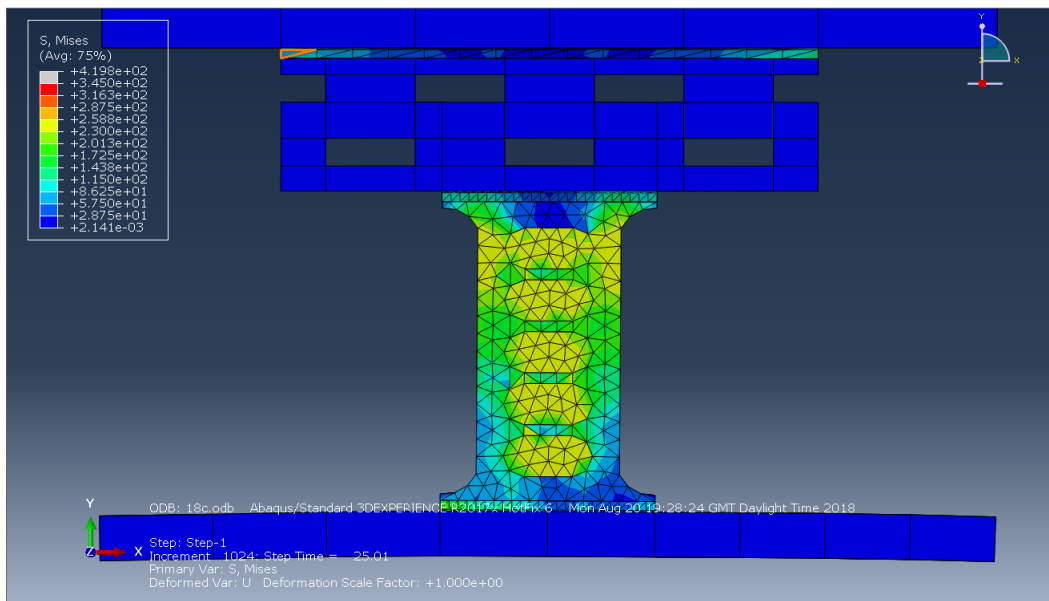


Figure 29. Von Mises stresses for the SLB connection Type 1

8. Influence of parameters

In order to understand which parameters of the test are the most relevant and how their geometry and position affect the results, many numerical analysis were done changing their dimensions as shown in table 6.

Table 6. Parameters variation

| Parameters variation | |
|-----------------------|--------------|
| Total height | ± 20 mm |
| Dissipative height | ± 2 mm |
| Width | ± 10 mm |
| Dissipative thickness | ± 1 mm |
| Position | ± 100 mm |

8.1. Influence of Total height, dissipative height, width, and dissipative thickness.

As displayed in Figure 30, usually when increasing or diminishing the volume of the SLB connections, its load capacity improves or deteriorates respectively; however, the increasing the height just worsen the whole performance of the SLB connections. It can be deduced that compact SLB connections have a better behaviour.

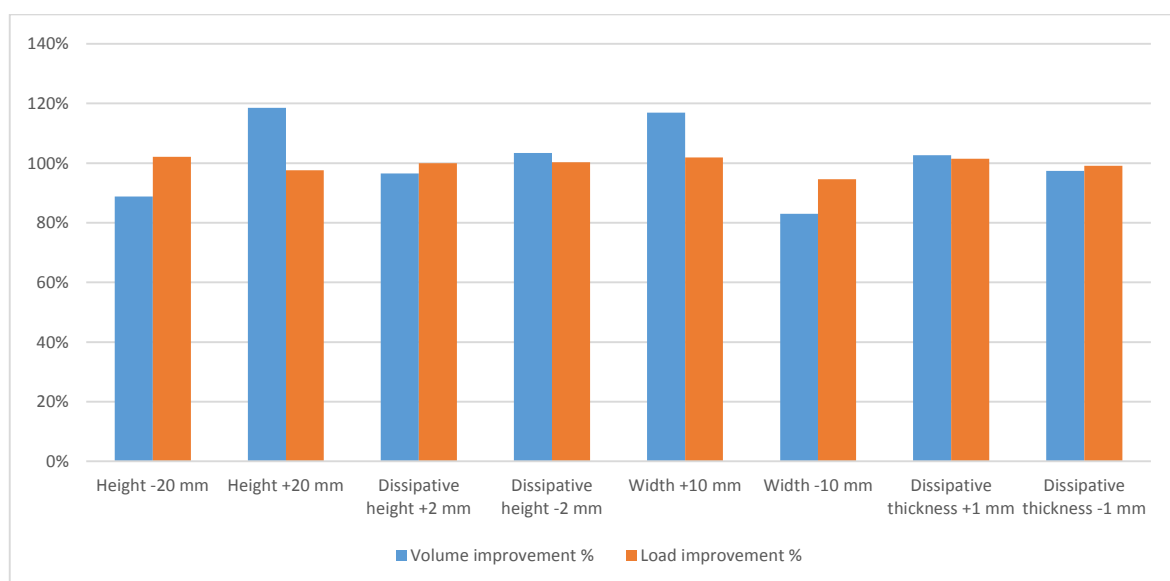


Figure 30. Influence of different parameters – numerical models (%)

8.2. Influence of horizontal position of SLB connections

As shown in Figure 31, the behaviour of the SLB connections can be improved by varying its horizontal position along the reaction wall. However, the improvement in behaviour is negligible due to low values.

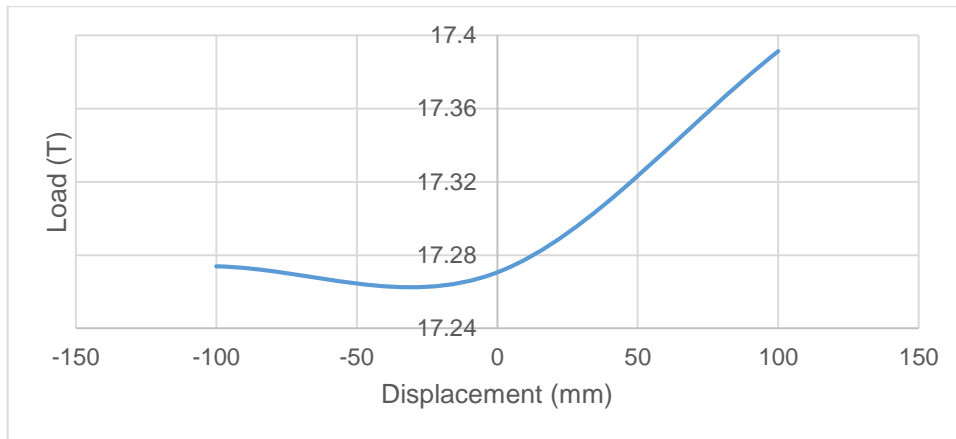


Figure 31. Influence of position – numerical models

8.3. Fixed supports

Furthermore, a model using fixed supports was implemented as shown in Figure 32, it displays that using good connections between the reaction wall and the SLB devices, the behaviour of the SLB connections is improved significantly, reaching values of 140% of the load capacity of the model using spring supports. Besides, there is a higher Von Mises stress distribution in the SLB connections reaching high plastic deformations as shown in Appendix C.

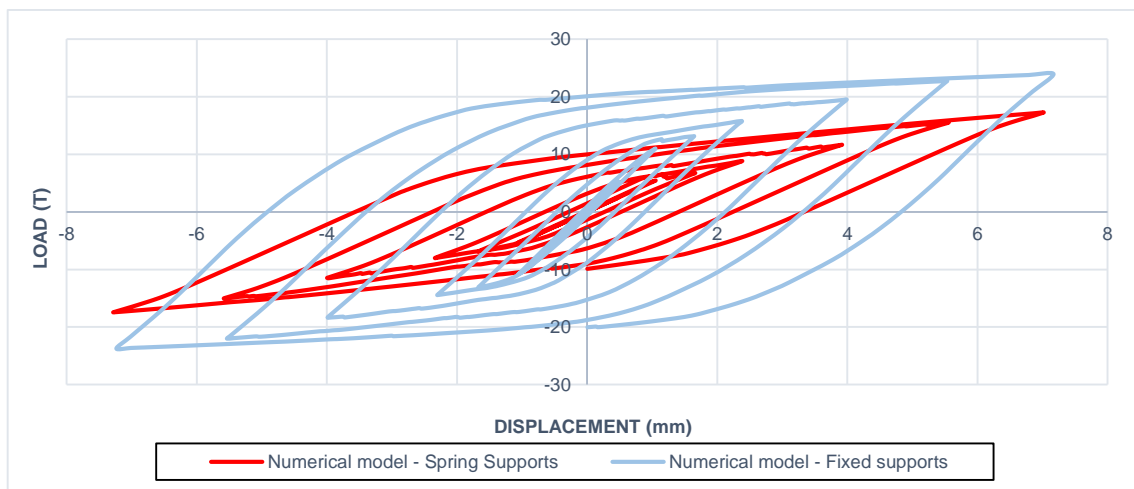


Figure 32. Load-Displacement relationship (Numerical model – spring supports / fixed supports)

9. Results and discussions

9.1.1. Concrete frame without SLB connections

Since the section was already cracked while being tested, the experimental results display a cracked behaviour of the section. Therefore, the proper way to validate the numerical model was using just the cracked section of the element, which means validating the model using its cracked stiffness.

9.1.2. Uncoupled frame with SLB connections type 1

Many parameters were varied to get the most effective way to improve the behaviour of the SLB connections, some of them do not have great influence on their response, meanwhile others display great amounts of energy dissipated such as fixed supports.

9.1.3. Uncoupled frame with SLB connections type 2

This specimen was not modelled since unexpected behaviour was conveyed during the test regarding that the connections were not good enough to let the SLB connections behave properly.

10. Conclusions and Recommendations

10.1. Conclusions

10.1.1. Numerical validation

The nonlinear FE models displayed good numerical correlations with the experimental results conveying well-shaped hysteretic curves. The test order influenced significantly the numerical validation of the frame without SLB connections since the columns were already cracked when tested. Therefore, the cracked stiffness of the concrete frame was used to validate the numerical model. Even though the meshing method was not the most accurate given by ABAQUS CAE due to the complex geometry of the SLB connection, it was sufficient enough to obtain a similar behaviour given by test; besides, the modelling of the reaction wall had to be replaced by linear springs in order to simulate its behaviour since there was not a good connection between the bottom plate of the SLB connections and the reaction wall, this lack of connectivity can be labelled as a relevant unforeseen mistake of the test setup.

10.1.2. Influence of dimensions

As seen in the results, usually while increasing the dimensions of the SLB connections, its behaviour is improved; however, while reducing the total height of the device, the SLB connection reaches higher values, which means that a compact device can display a better performance using less material; which translates as a cheaper device. On the other hand, it means that the reaction wall should be taller to fulfil the connection; therefore, higher costs might be considered.

10.1.3. Influence of horizontal position of SLB connections

It is important to get the right position of the SLB connections to obtain the most benefit. According to the tests, while distancing the devices from each other, their performance reaches higher values which means that higher moments occur; however, changing its position

provides a minimum improvement or degradation; therefore, it is not the most influential parameter.

10.1.4. Influence of supports

As seen in the results, using fixed supports instead of spring ones, provides better results being the most effective way to improve the whole behaviour of the structure. Fixed supports physically means that complete displacement and rotation restrictions are assumed. To achieve this in the test, the connection between the bottom plate of the device and the reaction wall must work perfectly; it is possible if the spaces left in the holes are filled with grout to improve the connection. Under this terms, it is possible to take advantage of the mechanical characteristics of the reaction wall since its stiffness can be considerate as infinite compared with the columns and SLB connections. On the other hand, the results may let to understand that probably using a reaction wall in the system is not the best technique; hence, using a different structural system such as steel braces might behave good enough to let the SLB connections dissipate high amounts of energy.

10.2. Recommendations for further action

This project considers lateral monotonic loads in order to evaluate the behaviour of SLB connections; nevertheless, other types of loads like seismic might be considered regarding that the numerical model is validated properly and displays a similar behaviour of the experimental test.

Besides, the SLB connections type 2 was not numerically modelled in this project; however, the experimental results of this part of the test might be used to model this the unexpected scenario in order to avoid it to happen again.

Finally, a linear dynamic equation may be considered in future researches in order to represent the whole behaviour of the test using a two degree-of-freedom system using the data results to validate it and estimate the damping capacity provided by the SLB connections.

References

- ASM International (2002) *Atlas of Stress-Strain Curves*. 2nd edn. United States of America: The Materials Information Society.
- Agico Group (2018) *ASTM A36 Carbon Structural Steel Plate*. Available at: <http://www.steels-supplier.com/steel-standard/astm-a36-carbon-structural-steel-plate.html> (Accessed: 10 August 2018).
- Aguiar, R. (2002) *Sistema de computación CEINCI3 para evaluar daño sísmico en los Países Bolivarianos [Computational system CEINCI3 for evaluating seismic damage in Bolivarian countries]*. Quito: Escuela Politécnica del Ejército.
- Ahmed, A. (2014) 'Modeling of a reinforced concrete beam subjected to impact vibration using ABAQUS'. *International journal of civil and structural engineering*, 4(3), pp. 227-236.
- Bhaskaran R. (2016) *A Hands-on Introduction to Engineering Simulations*. Available at: <https://courses.edx.org/courses/course-v1: CornellX+ENGR2000X+1T2018/course/> (Accessed: 03 September 2018).
- Boza, Z., and Galan, D. (2013) *Diseño de un edificio aporricado con disipadores en arreglo chevrón [Design of a framed building with chevron dissipators]*. Unpublished dissertation. Lima: Pontificia Universidad Católica del Perú.
- Bozzo, L. (2017) *Luis Bozzo [Facebook][video]* October. Available at: http://www.facebook.com/luis.bozzo.54/videos/vb.100003930148975/992994600841535/?type=2&video_source=user_video_tab (Accessed: 25 July 2018).
- Bozzo, L., Cahís, X., and Torres, L. (1998) 'A shear type energy dissipator for the protection of masonry infill walls', *Sixth US national conference on earthquake engineering*. Seattle, Washington. May 31 - June 4. Earthquake Engineering Research Institute
- Bozzo, L. and Gaxiola, G. (2015) 'El concepto "rigido-flexible-dúctil" y las conexiones SLB' [The concept "rigid-flexible-ductil" and the SLB connections]. *Twentieth national congress of seismic engineering*. Acapulco. 25 - 28 November.
- Broujerdian, V. (2016) 'Nonlinear Finite Element Modeling of Shear-Critical Reinforced Concrete Beams using a set of interactive constitutive laws', *International Journal of Civil Engineering*, 14(8), pp. 1-30.
- Cahis, X., Bozzo, L., and Torres, L. (1998) 'Experimental studies of various innovative energy dissipation devices'. *Proceeding of the Eleventh European Conference on Earthquake Engineering*. 6 - 11 September. Paris: Rotterdam : A.A. Balkema.
- Cahis, X., Torres, L., and Bozzo, L. (2000) 'An innovative elastoplastic energy dissipator for the structural and non-structural building protection'. *Proceeding of the twelfth World Conference on Earthquake Engineering*. 30 January - 4 February. Auckland. Upper Hutt: New Zealand Society for Earthquake Engineering.
- Chambilla, A. (2015) *Diseño estructural del centro de salud de Chen-Chen utilizando disipadores por plastificación de metales [Structural design of the Chen-Chen medical care unit using metal plastifying dissipators]*. Unpublished dissertation. Moquegua: Universidad José Carlos Mariátegui.

Dassault Systèmes Simulia Corp. (2010) *Abaqus Analysis User's Manual*. Available at: <https://www.sharcnet.ca/Software/Abaqus610/Documentation/docs/v6.10/books/usb/default.htm?startat=pt05ch20s06abm38.html> (Accessed: 08 August 2018).

De la Llera, J. C. (2010) *Protección sísmica de estructuras en Chile: Pasado, presente y futuro [Seismic protection of structures in Chile: Past, present and future][Slides]*. 12 July. Santiago: Pontificia Universidad Católica de Chile.

Foti, D., Bozzo, L., and Lopez-Almansa, F. (1998) 'Numerical efficiency assessment of energy dissipaters for seismic protection of buildings', *Earthquake engineering & structural dynamics*, 27(6), pp. 543-556.

Hurtado, F., and Bozzo, L. (2008) 'Numerical and experimental analysis of a shear-link energy dissipator for seismic protection'. *The fourteenth world conference on earthquake engineering*. 12 - 17 October. Beijing: World Conference on Earthquake Engineering.

Instituto de Ingenieria UNAM (2017) *Ensayo experimental de un marco de concreto reforzado equipado con disipadores de energía sísmica "SLB" [Experimental test of a reinforced concrete frame equiped with seismic energy dissipators "SLB"]*. Ciudad de Mexico: Universidad Nacional Autónoma de México.

Nuzzo, I., Losanno, D., Serino, G., and Bozzo, L. (2015) 'Simplified Nonlinear Analysis: Application to Damper-Braced Structures'. *Proceedings of the Fifteenth International Conference on Civil, Structural and Environmental Engineering Computing*. Stirlingshire: Civil-Comp Press.

Nuzzo, I., Losanno, D., Serino, G., and Bozzo, L. (2015) 'A Seismic-resistant Precast R.C. System equipped with Shear Link Dissipators for Residential Buildings', *International Journal of Civil and Structural Engineering- IJCSE*, 2(1), pp. 270-275.

Oviedo, R. (2008) *Dispositivos pasivos de disipación de energía para diseño sismorresistente de estructuras [Energy dissipating pasive devices for seismicresistant design of structures]*. Unpublished dissertation. Lima: Universidad Nacional de Ingeniería.

Verma, A., Gupta, A., and Nath, B. (2017) 'Base isolation system: a review', *International Journal of Engineering Science Invention*, 6(9), pp. 43-46.

Appendix A: Engineering Simulation

Professor Bhaskaran (2016) from Cornell University explains the fundamentals of engineering simulation through the course “A Hands-on Introduction to Engineering Simulations” in which he calls the Finite Element software a “black box” since practically users input geometry, define mesh, boundary conditions, material properties and, consequently, the software outputs results which commonly are represented by colours. Colours can mislead users to accept values that are not right or accurate enough.

In order to solve a physical problem, it must be clear what the inputs are considering that the software is not solving a physical problem rather than a mathematical one of the physical problem based on equilibrium or conservation laws. Besides, it is not necessary to obtain selected variables of every node of the structure, specific points must be selected.

Therefore, in every study case, it is necessary to go through a pre-analysis to help to see what is under the “black box”. The first question to ask in the pre-analysis is what mathematical model is being solved considering the physical principles implied and embedded assumptions. Next, it is important to consider the numerical solution strategy being used, the introduced errors and how to minimize them. Finally, the last step consists of hand calculations of expected results or trends. All of these steps form the basis for verification and validation.

Verification and validation are systematic processes of checking results. Verification implies the question whether or not the model was solve right by checking if the results are consistent with the mathematical model; next, if whether the level of numerical errors is acceptable; moreover, if whether there is a reasonable comparison with hand calculations.

On the other hand, validation, which is the systematic process applied in this research, implies the question whether or not the right model was solved checking if the mathematical model used is a reasonable representation of the physical problem. In this step is where numerical results are compared directly with experimental data according to the physical setup.

Appendix B: Mesh sensitivity

In order to obtain good enough results through the use of the software ABAQUS CAE, the mode has been subjected to a number of analysis in order to see what elements affect most the behaviour of the whole structure and how their mesh distributions affect the accuracy taking into account the computational effort.

Therefore, the used mesh in this research is compared with finer ones in steel elements, and another using finer mesh in steel and concrete elements conveying very similar results with a small error 0.6%. The used mesh distribution in this research project is applied due to its manageable computational time.

Besides, figure 34 displays that using a finer mesh distribution in the steel elements next to the SLB connections, there is no appearance of Von Mises stresses which can be interpreted as an infinitive rigid behaviour.

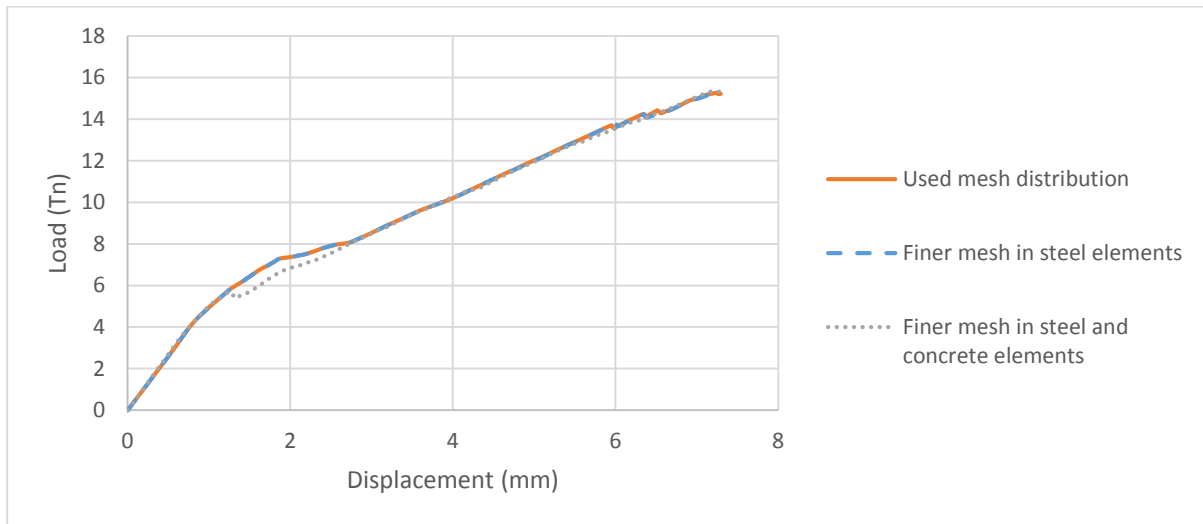


Figure 33. Mesh distribution comparison

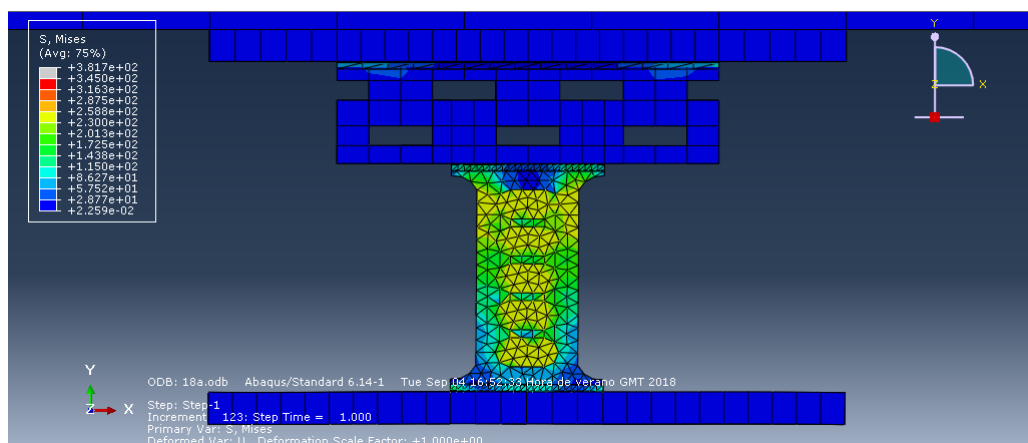


Figure 34. Von Mises stress distribution - finer mesh in steel elements

Appendix C: Von Mises stress distribution in all studied specimens.

Table 7. Von Mises stress distribution in all specimens (Time interval: 25 sec)

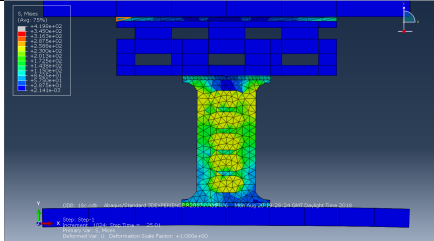
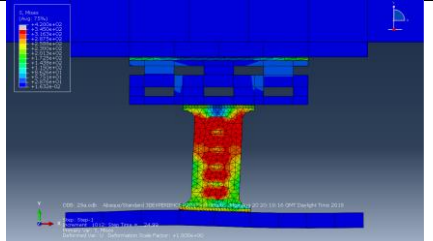
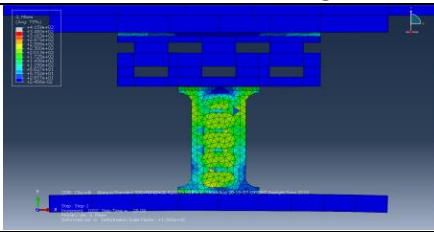
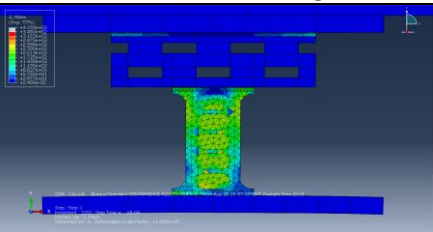
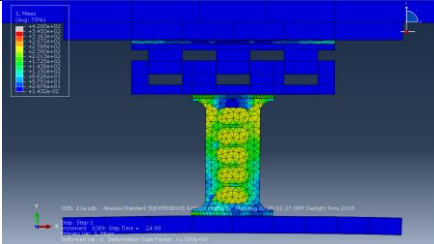
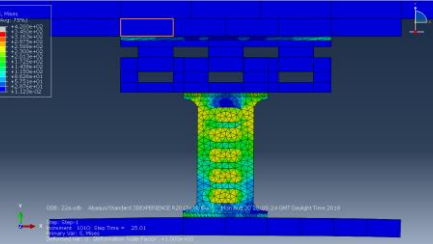
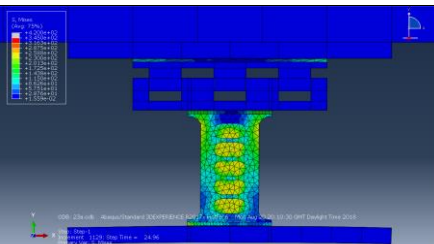
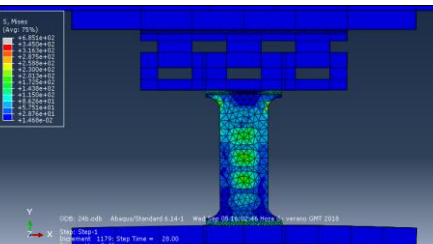
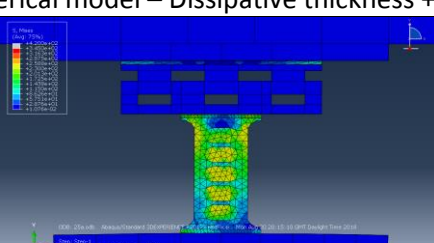
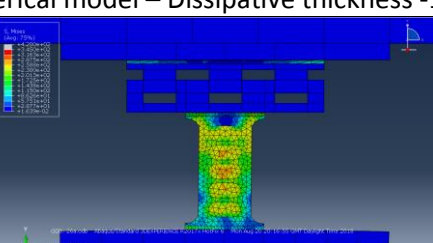
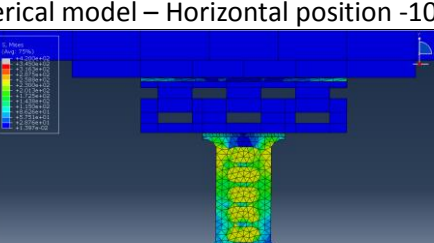
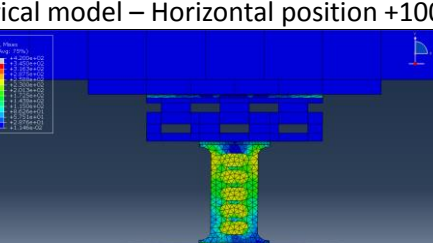
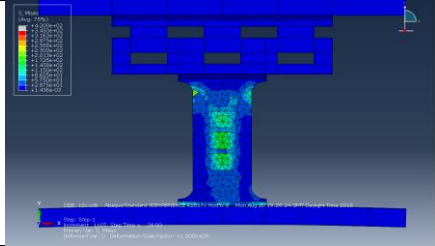
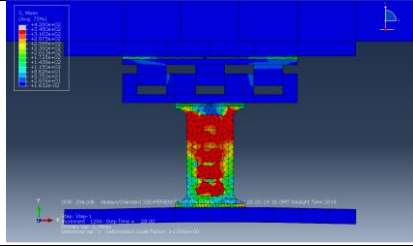
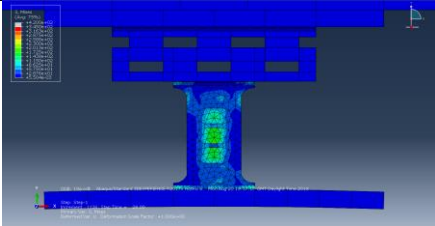
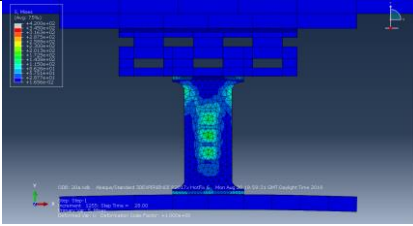
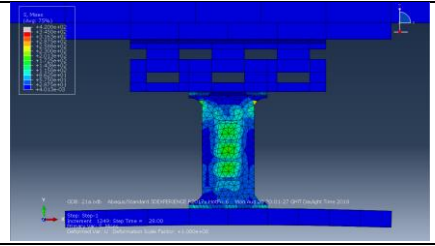
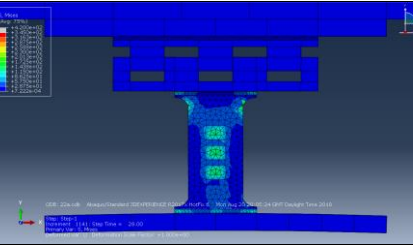
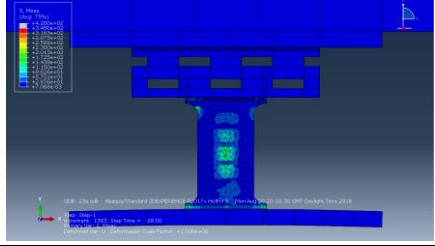
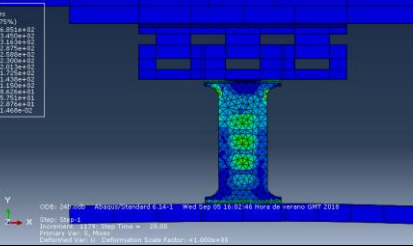
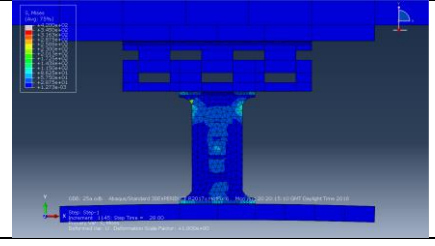
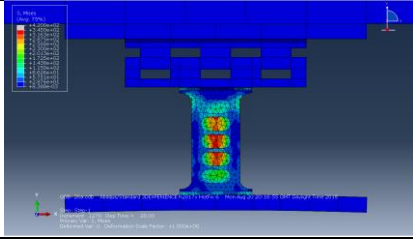
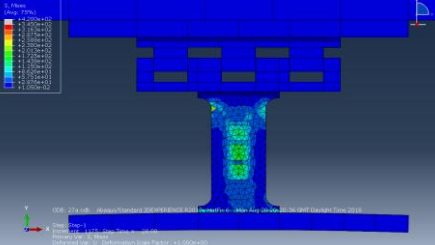
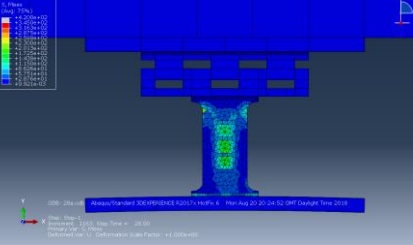
| | |
|--|---|
| <p>Validated numerical model</p>  | <p>Numerical Model – Fixed supports</p>  |
| <p>Numerical model – Total height -20 mm</p>  | <p>Numerical model – Total height +20 mm</p>  |
| <p>Numerical model – Dissipative height +2 mm</p>  | <p>Numerical model – Dissipative height -2 mm</p>  |
| <p>Numerical model – Total width +10 mm</p>  | <p>Numerical model – Total width -10 mm</p>  |
| <p>Numerical model – Dissipative thickness +1 mm</p>  | <p>Numerical model – Dissipative thickness -1 mm</p>  |
| <p>Numerical model – Horizontal position -100 mm</p>  | <p>Numerical model – Horizontal position +100 mm</p>  |

Table 8. Von Mises stress distribution in all specimens (Time interval: 28 sec)

| Validated numerical model | Numerical Model – Fixed supports |
|---|--|
|  |  |
| Numerical model – Total height -20 mm | Numerical model – Total height +20 mm |
|  |  |
| Numerical model – Dissipative height +2 mm | Numerical model – Dissipative height -2 mm |
|  |  |
| Numerical model – Total width +10 mm | Numerical model – Total width -10 mm |
|  |  |
| Numerical model – Dissipative thickness +1 mm | Numerical model – Dissipative thickness -1 mm |
|  |  |
| Numerical model – Horizontal position -100 mm | Numerical model – Horizontal position +100 mm |
|  |  |